High-precision (p,t) reaction measurement to determine ^{18}Ne$(\alpha,p)^{21}$Na reaction rates

A. Matic,[*] A. M. van den Berg, M. N. Harakeh, and H. J. Wörtche
Kernfysisch Versneller Instituut, University of Groningen, Zernikelaan 25, NL-9747 AA Groningen, The Netherlands

G. P. A. Berg, M. Couder, J. L. Fisker,[†] J. Görres, P. LeBlanc, S. O'Brien, and M. Wiescher
Department of Physics and the Joint Institute for Nuclear Astrophysics, University of Notre Dame, Notre Dame, Indiana 46556, USA

K. Fujita, K. Hatanaka, Y. Sakemi, Y. Shimizu,[‡] Y. Tameshige, A. Tamii, and M. Yosoi
Research Center for Nuclear Physics, Osaka University, Ibaraki, Osaka 560-0047, Japan

T. Adachi, Y. Fujita, and Y. Shimbara
Department of Physics, Osaka University, Toyonaka, Osaka 560-0043, Japan

H. Fujita
School of Physics, University of the Witwatersrand, P. O. Wits, Johannesburg 2050, South Africa

T. Wakasa
Department of Physics, Kyushu University, Fukuoka 812-8581, Japan

P. O. Hess
Institute of Nuclear Sciences, Universidad Nacional Autonoma de Mexico (UNAM), Mexico

B. A. Brown and H. Schatz
National Superconducting Cyclotron Laboratory, Michigan State University, East Lansing, Michigan 48824, USA
(Received 2 December 2008; published 16 November 2009)

x-ray bursts are identified as thermonuclear explosions in the outer atmosphere of accreting neutron stars. The thermonuclear runaway is fueled by the αp process that describes a sequence of (α,p) reactions triggered by the ^{18}Ne$(\alpha,p)^{21}$Na breakout reaction from the hot CNO cycles. We studied the level structure of the compound nucleus ^{22}Mg by measuring the ^{24}Mg$(p,t)^{22}$Mg reaction at the Grand Raiden spectrometer at Research Center for Nuclear Physics, Osaka. A large number of α-unbound states was identified and precise excitation energies were determined. Based on shell model and α-cluster model calculations we predict the level parameters for determining the stellar reaction rate of ^{18}Ne$(\alpha,p)^{21}$Na for a wide temperature range. x-ray burst simulations have been performed to study the impact of the reaction on the x-ray burst luminosity.

DOI: 10.1103/PhysRevC.80.055804 PACS number(s): 25.40.Hs, 26.30.Ca, 26.50.+x, 27.30.+t

I. INTRODUCTION

x-ray bursts belong to the most fascinating of astrophysical phenomena. The x-ray burst is characterized by a repeated sudden increase of x-ray emission within only a few seconds to a total energy output of about 10^{40} ergs. The recurrence time for single bursts can range from hours to days. These bursts are explained in the framework of the *thermonuclear flash model* as thermonuclear explosions in the atmosphere of an accreting neutron star in a close binary system [1,2]. When critical values for density and temperature are reached in the neutron star atmosphere, the freshly accreted hydrogen and helium ignites the hot, β-limited CNO cycles (HCNO) [3,4]. With the ignition of the triple-α process, fresh CNO catalyzing material is produced causing an increase in temperature [3]. When a critical temperature is reached, breakout from the hot CNO cycles occurs via α-capture processes on the HCNO waiting point nuclei ^{15}O and ^{18}Ne feeding the rp process [5–7]. The ^{14}O$(\alpha,p)^{17}$F reaction is often erroneously labeled as a CNO breakout reaction but it only transfers material from the first hot CNO cycle to the second one, to be subsequently redistributed toward ^{15}O by the reaction sequence ^{17}F$(p,\gamma)^{18}$Ne$(\beta^+\nu)^{18}$F$(p,\alpha)^{15}$O. The reaction rates of both breakout reactions are critical for the ignition and the fueling of the rp process. In both cases, the reaction rates have not been experimentally determined and carry significant uncertainties. This translates directly into uncertainties for the model predictions of x-ray bursts [7–11].

The reaction rates for ^{15}O$(\alpha,\gamma)^{19}$Ne and ^{18}Ne$(\alpha,p)^{21}$Na are dominated by resonance contributions. Direct capture contributions are negligible [12,13]. The uncertainties are mainly caused by the errors in the excitation energies and

[*]Present address: Forschungszentrum Dresden−Rossendorf, Postfach 510119, 01314 Dresden, D-01328 Dresden, Germany.
[†]Present address: Lawrence Livermore National Laboratory, P.O. Box 808, L-414, Livermore, CA 94550, USA.
[‡]Present address: Center for Nuclear Study, University of Tokyo, Wako, Saitama 351-0198, Japan.

the strengths $\omega\gamma$ of the resonance contributions. Recent indirect measurements of the level parameters of ^{19}Ne strongly reduced the uncertainties in the critical resonance parameters and therefore of the reaction rate of ^{15}O$(\alpha,\gamma)^{19}$Ne [14–16]. A direct measurement to verify this reaction rate remains important but requires higher ^{15}O beam currents than presently available [17].

The uncertainty in the ^{18}Ne$(\alpha,p)^{21}$Na reaction rate is considerable. The first estimate of the rate was made a decade ago [13] and was based on rather limited experimental data of the level structure of the compound nucleus ^{22}Mg above the α threshold at 8.14 MeV. Comparison with the mirror nucleus ^{22}Ne indicates a rather high level density. This suggests that a statistical approach might be justified for a first estimate. However, α capture on ^{18}Ne selectively populates natural-parity states and the resonance density will be smaller than the level density in a statistical-model approach. A wide range of experiments were performed to selectively populate α-unbound natural-parity states in ^{22}Mg. The preferred method was using transfer reactions such as ^{12}C(^{16}O,^{6}He)^{22}Mg [18], ^{25}Mg(^{3}He,^{6}He)^{22}Mg [19], and ^{24}Mg(^{4}He,^{6}He)^{22}Mg [20] to determine the excitation energies of possible resonance states with an experimental uncertainty of $\pm$20 keV. This uncertainty can introduce significant errors in the calculated stellar rates. Complementary to these indirect studies of resonance states, radioactive beam experiments were performed at the Louvain la Neuve radioactive beam facility to probe directly the resonance strengths [21,22]. In these two experiments seven [21] and eight [22] resonance states at excitation energies above 10 MeV were identified with accuracies of 50 and 140 keV, respectively. However, the low ^{18}Ne beam intensities limited the direct measurements to these few high-energy resonances.

Based on all these experimental data, first estimates have been made for the reaction rate by using Eq. (1),

$$N_A\langle\sigma v\rangle_{\rm res} \propto (kT)^{-3/2}\sum_i(\omega\gamma)_i \times \exp\left(-\frac{E_i}{kT}\right), \qquad (1)$$

where E_i is the resonance energy in the center-of-mass system and $(\omega\gamma)_i$ is the resonance strength of the contributing compound nucleus state i,

$$(\omega\gamma)_i = \frac{(J_i+1)}{2}\frac{\Gamma_\alpha\times\Gamma_p}{(\Gamma_\alpha+\Gamma_p+\Gamma_\gamma)}, \qquad (2)$$

where J_i is the resonance spin and Γ_α, Γ_p, and Γ_γ the α, proton, and γ partial widths, respectively. These estimates, however, still carry large uncertainties.

We have performed an independent measurement of the ^{24}Mg$(p,t)^{22}$Mg reaction at the RCNP facility in Osaka, Japan, to investigate the level structure in ^{22}Mg with improved accuracy. In this work we have used the high-resolution Grand Raiden spectrometer at RCNP [23] to measure energy levels up to 13 MeV with a resolution of 13 keV. Several levels were seen for the first time with errors significantly better than 10 keV (except for states with low statistics). Above 10 MeV excitation energy the uncertainties are of the order of 10 keV. The improved accuracies of the excitation energies for levels above the α threshold were used to calculate rates of the ^{18}Ne$(\alpha,p)^{21}$Na reaction with smaller uncertainties than previously possible. The partial widths for the resonance states were estimated based on shell-model calculations for single-particle and α-cluster structures in the $A = 22$ system. The shell-model calculations were complemented with α-cluster model calculations in the framework of the semimicroscopic algebraic cluster model (SACM) [24,25] to determine the overall α-cluster strength distribution above the α threshold. The astrophysical implications of these stellar rates are discussed and compared to previous calculations.

II. EXPERIMENTAL SETUP

To identify resonance levels in ^{22}Mg, the ^{24}Mg$(p,t)^{22}$Mg reaction was measured using the high-resolution spectrometer Grand Raiden (GR) at the Research Center for Nuclear Physics (RCNP) of Osaka University. A 98.7-MeV proton beam from the ring cyclotron was transported via the "fully dispersion-matched" WS beam line [26] to the target chamber in front of the spectrometer. The new WS beam line is designed [27] to fulfill all required matching conditions: focus condition, lateral-dispersion matching, and angular-dispersion matching. By using this unique method, the spectral resolution is not limited by the energy spread of the beam but can be as good as the resolving power of the spectrometer. In our experiment, the resolution was mainly limited by the target thickness, i.e., the energy-loss difference between protons and tritons in the target. The thickness of 0.82 mg/cm^2 of the ^{24}Mg target was a compromise between the best possible resolution and a sufficient count rate. We achieved an unprecedented resolution of 13 keV (FWHM) for a (p,t) experiment with a proton beam of about 100 MeV incident energy.

The ^{24}Mg target with an isotopic enrichment of 99.6% was self-supporting but contained ^{12}C and ^{16}O impurities. For the identification and subtraction of events from these contaminants, a 1-mg/cm^2 thick ^{12}C target and a 1-mg/cm^2 thick Mylar target were used. Due to the strongly negative Q value for the ^{24}Mg$(p,t)^{22}$Mg reaction and the high enrichment of the ^{24}Mg target other impurities are strongly suppressed. No such peaks were observed in the low-energy region of the spectrum and, therefore, we assume that all peaks at higher excitation energies correspond to levels in ^{24}Mg.

The outgoing tritons were momentum analyzed by the GR spectrometer with a very high momentum resolving power $p/\Delta p = 37000$ [23]. The detector system consisted of two multi-wire drift chambers (MWDC) that are sensitive in the horizontal and vertical directions, followed by three plastic scintillators for timing and particle-identification purposes. To accurately reconstruct the scattering angles at and near 0°, the *overfocus* mode [28] was employed. The angle calibration measurements were performed with a multihole aperture (sieve-slit) at the entrance of the spectrometer.

III. EXPERIMENTAL RESULTS

Energy levels in ^{22}Mg were measured up to an excitation energy of about 13 MeV. Grand Raiden has a momentum

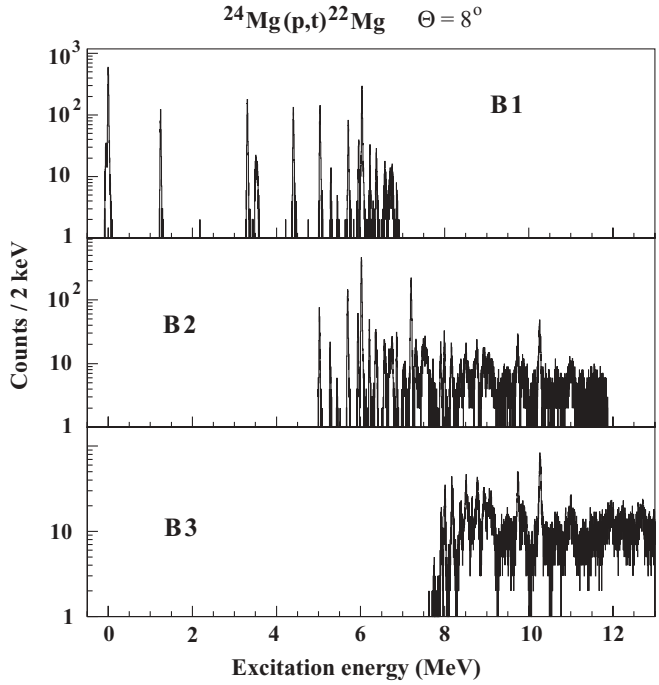

FIG. 1. The measured ^{24}Mg$(p,t)^{22}$Mg spectra at 8° and 98.7 MeV incident proton energy are shown at three magnetic-field settings, B1, B2, and B3.

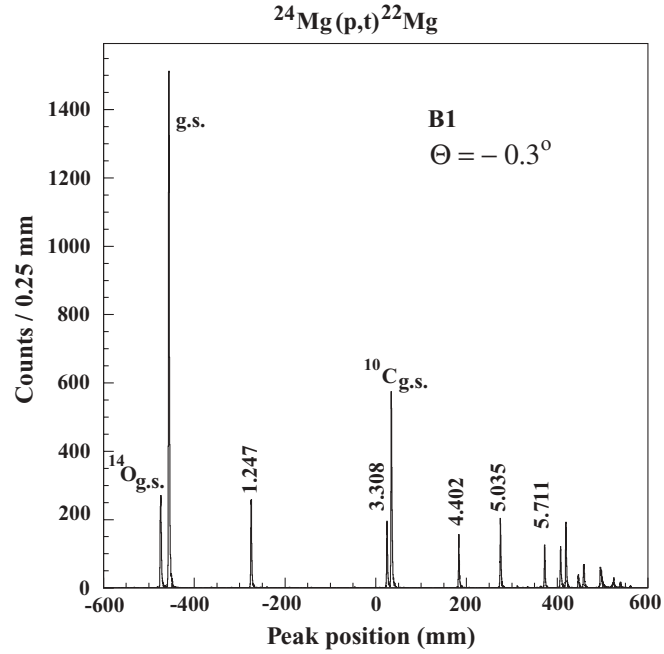

FIG. 2. The spectrum of the ^{24}Mg$(p,t)^{22}$Mg reaction measured at 98.7 MeV incident energy and the magnetic-field setting B1 is shown. Excited states used in the calibration are marked by their excitation energies in MeV.

acceptance of 5% [23]. This is too small to cover the excitation energy range of interest with one magnetic-field setting. Therefore, experiments were performed at three different magnetic-field settings, B1, B2, and B3, chosen so that there were overlapping portions of the spectra, as can be seen in Fig. 1. This allows for accurate calibration at high excitation energies. Well-known states of natural parity at lower excitation energies were used to calibrate the focal plane.

Measurements were performed at three different spectrometer angles, −0.3°, 8°, and 17° to help with the identification of impurity lines by their kinematic shift. We subtracted the ^{10}C and ^{14}O impurity lines that were measured using carbon and Mylar targets. The intensity of these impurity lines were normalized to the separated ^{10}C and ^{14}O ground-state lines that can be seen in the ^{22}Mg spectrum in Fig. 2.

A more detailed description of experimental conditions and procedures can be found in the Ph.D. thesis of A. Matic [29].

A. Reference data

Before presenting our results, we need to discuss a discrepancy between the data published by Seweryniak *et al.* [30] and Bateman *et al.* [31] and summarized in an earlier compilation of Endt [32] (see Table I). The levels indicated with the superscript "a" are from Endt and were used by Bateman *et al.* for their calibration. Differences exist between the following values of Refs. [30] and [31] [4.4020(3)–4.3998(42), 5.7110(10)–5.7139(12)], although the first two values agree within the error bars. It is important to mention that Bateman *et al.* used only two previously known ^{22}Mg levels, at 5.0370

TABLE I. Energy levels of ^{22}Mg from the literature used in the present analysis (ground state = g.s.). Data from Seweryniak *et al.* [30] are compared with those from Bateman *et al.* [31] and Caggiano *et al.* [19]. All energies are given in MeV.

Ref. [30]	Ref. [31]	Ref. [31][b]	Ref. [19]
g.s.*	–	–	g.s.[a]
1.24718(3)*	–	–	1.2463[a]
3.30821(6)*	–	–	3.3082[a]
4.4020(3)*	4.3998(42)	4.4013(42)	4.4009[a]
5.0354(5)*	5.0370(14)[a]	5.0362(14)	5.033(7)
5.0893(8)	5.0897(17)	5.0887(17)	5.094(6)
5.2931(14)	5.2957(16)	5.2939(16)	5.301(4)
5.2960(4)	–	–	–
5.4524(4)	5.4543(16)	5.4519(16)	5451(5)
5.7110(10)*	5.7139(12)[a]	5.7106(12)	5.7139[a]
–	5.9619(25)	5.9577(25)	–
–	6.0458(30)	6.041(3)	6.051(4)
–	6.2464(51)	6.241(5)	6.246(4)
6.2542(3)	6.2464(51)	6.241(5)	6.246(4)
–	6.3226(60)	6.3170(60)	6.329(6)
–	6.613(7)	6.606(7)	6.616(4)
–	6.787(14)	6.780(14)	6.771(5)

*Levels with an asterisk were used in the present calibration.
[a]Level energies indicated with superscript a were used by Bateman *et al.* and Caggiano *et al.* in their calibration.
[b]The superscript b indicates corrected values as explained in Sec. III A.

and 5.7139 MeV, for the calibration of their (p,t) spectra. But the 5.7139-MeV level is in discrepancy with the corresponding level listed in Ref. [30] and the 5.037-MeV level has an error three times larger than the corresponding level listed in Ref. [30]. We corrected the excitation-energy calibration of Bateman *et al.* by using a simple linear function. The corrected excitation energies are shown in the third column of Table I. The new calibration gives a better agreement between the excitation energies of Bateman *et al.* and Seweryniak *et al.* These excitation energies will be compared with our results rather than those from Ref. [31].

B. Fits of the spectra

The peak positions were determined by using two different methods. The natural level widths of states below the proton-emission threshold of 5.5042 MeV are much smaller than the instrumental width. Therefore, we used the measured peak shape of the first 2^+ state to fit the low-lying levels with the peak positions and the heights as free parameters. The levels above the proton-emission threshold were fitted including the widths of the peaks to accommodate the natural width that increases above the proton threshold. No background was assumed for low excitation energies. For excitation energies higher than 7 MeV we adopted a constant background.

When using detectors where the particle energies are measured by statistical processes the peak shapes can usually be fitted well by symmetrical Gaussian functions. Because the transmission through a spectrometer can include higher-order aberrations of the ion optics, the peak shapes are typically asymmetric. This can be seen most clearly in the large peaks of the spectra above the proton threshold shown below where the peaks are asymmetric with noticeable tails. Therefore, our fit functions consist of a combination of a Gaussian function with high and low energy exponential tails. The fitting parameters were obtained empirically by fitting the well separated peaks at 1.247 MeV, 5.711 MeV, and 7.2183 MeV for the corresponding excitation energy regions. All peak fits are dominated by the Gaussian component of the peak and, therefore, we have taken the center of the Gaussian component as the peak position. To test the error this introduces in the calibration of the excitation energies, we have compared these positions with positions obtained from fits using a pure Gaussian function. The differences were at most 0.6 keV. Because this is smaller than other errors in the energy calibration this error was neglected. For details of the fitting procedure including the exact functions and examples of fitted peaks, see Ref. [29].

C. Calibration

The best possible energy calibration is important for the accuracy of the stellar rate calculations. For this reason it is described here in some detail. The focal-plane position of magnetic spectrometers like GR has in first order a linear relation to the momentum p of the analyzed ion with a small quadratic term that was included in the calibration function. This calibration function is determined using the well-known ground-state masses of the target nuclei and the excitation energies of the lowest-lying states. The stability of the spectrometer dipole field B was monitored over the duration of a measurement of a spectrum with a NMR probe and was always constant within a precision of better than $\Delta B/B = 10^{-5}$. This does not contribute to the error of the calibration. However, if the spectrometer magnetic field is changed, e.g., to measure the higher-excitation-energy region, the precision of the calibration is lost due to "differential hysteresis" of the magnetic field, despite the fact that the NMR probe allows us to measure the field in one location to a precision of $\Delta B/B = 10^{-5}$. "Differential hysteresis" means that the magnetic field of a large dipole magnet does not scale in all locations linearly as measured by the NMR probe to this precision when the magnetic field is changed. Therefore, when changing the magnetic field to measure higher excitation energies, we have measured spectra with an overlap of several peaks to be able to determine the scaling factor more precisely. The precision of the calibration also depends on the stability of the cyclotron beam. The momentum distribution of the beam was measured and minimized using a faint achromatic beam line tune and the spectrometer [33]. The flat top RF cavity was used to minimize the momentum width of the beam. Short-term stability of the beam over several hours is well maintained, but gradual beam-energy shifts of the order of a few tens of keV are observed in direct correlation with the cooling water temperature that was, for this reason, constantly monitored. The shift in beam energy can readily be seen in the spectrum as shift of the peaks with time. The data were analyzed in time segments of the order of 1 h and then shifted to line up the larger peaks to compensate for this effect. The resulting corrected spectra were then calibrated. The absolute beam energy was determined to be 98.7 MeV $\pm$0.1 MeV by eliminating differences due to kinematic effects for the calibrations of the target and the carbon and oxygen impurities. This energy uncertainty of the incident beam energy causes an error of less than 0.1 keV in the calibration of the excitation energies. To achieve the best possible resolution for the (p,t) spectra, software corrections were performed as outlined by Yosoi [34] to compensate for kinematic effects and optical aberrations. The experiment was performed in overfocus mode to achieve good angular resolution for GR at 0° and sieve-slit measurements [28] were made to calibrate target coordinates as a function of focal-plane coordinates. To eliminate residual effects of kinematics and optical aberrations we made cuts on the horizontal angle $-0.6^\circ < \theta_{\rm tg} < 0.4^\circ$ and the vertical angle $-1.5^\circ < \phi_{\rm tg} < 1.5^\circ$.

For the momentum calibration of the outgoing tritons, we used the new high-precision γ-spectrometry data of Ref. [30] studied via ^{12}C(^{12}C,2$n\gamma$)^{22}Mg. In the calibration, we used the ground state and five strongly populated natural-parity states indicated by an asterisk in the second column of Table I and by their excitation energies in Fig. 2. The ground states of ^{10}C and ^{14}O from target impurities are also labeled in the figure.

IV. ADOPTED ENERGY LEVELS

In the following we will discuss the measured level energies and compare them with previous results. The levels below the proton threshold are well known and are used for the

TABLE II. Excitation energies and adopted spin parities of the states below 5.711 MeV in ^{22}Mg including the states used in our energy calibration (ground state = g.s.).

J^{π} [a]	Present work (p,t)	Ref. [30] ^{12}C(^{12}C,2n)^{22}Mg(γ)	Ref. [31] (p,t)	Ref. [19] (^{3}He,^{6}He)	Ref. [38] (^{3}He,n)	Ref. [18] (^{16}O,^{6}He)	Adopted present
0^+	g.s.*	g.s.	–	g.s.[b]	g.s.	g.s.[b]	g.s.
2^+	1.24718*	1.24718(3)	–	1.2463[b]	1.244(32)	1.2463[b]	1.24718(3)
4^+	3.30821*	3.30821(6)	–	3.3082[b]	3.269(50)	3.3082[b]	3.30821(6)
2^+	4.4020*	4.4020(3)	4.4013(42)	4.4009[b]	4.378(35)	4.408(12)[b]	4.4020(29)
2^+	5.0354*	5.0354(5)	5.0362(14)	5.033(7)	5.032(30)	5.029(12)[b]	5.0346(5)
1^+[c]	(5.092(5))	5.0893(8)	5.0887(17)	5.094(6)	5.130(35)	–	5.0893(8)
4^+[c]	5.2947(23)	5.2931(14)	5.2939(16)	5.301(4)	5.286(30)	5.272(9)	5.2938(10)
2^-[c]	–	5.2960(4)	–	–	–	–	5.2960(4)
3^+[c]	5.454(4)	5.4524(4)	5.4519(16)	5.451(5)	5.433(25)	–	5.4524(4)
2^+	5.7110*	5.7110(10)	5.7106(12)	5.7139[b]	5.699(20)	5.711(13)[b]	5.7101(5)

*An asterisk indicates levels from Ref. [30] used in our calibration.
[a]Spin-partity values J^{π} in the first column are from compilation Ref. [35] except where labeled superscript c.
[b]Level energies used for calibration in previous articles. Data in the fourth column are the corrected data of Bateman *et al.* [31] as explained in the text. All energies are in MeV.
[c]More recently determined by Seweryniak *et al.* Ref. [30].

momentum calibration of the spectrometer. Subsequently, we will discuss the levels between the proton and α thresholds where our high resolution allowed to clarify several uncertainties and to identify new levels. The focus of this study is on levels above the α threshold that will be discussed in the context of possible resonances in ^{22}Mg that play a role in the ^{18}Ne$(\alpha,p)^{21}$Na reaction. The level parameters will be presented in measured spectra (Figs. 3–6), level schemes (Figs. 7–10), and Tables (Tables II–V). To avoid repetition, we summarize here notations and procedures that are used in these figures and tables. Energy levels marked by an asterisk are used in our calibration. Level parameters in parentheses are tentative assignments. "Present energies" are the results of our measurements. "Adopted level" parameters are used in our rate calculations and are derived using our excitation energies and parameters from the literature. Where measurements were performed at several angles (-0.3°, 8°, and 17°) we identified levels only when they were observed at least at two different angles. The excitation energy of a level was determined at the angle where this level was strongly excited and clearly separated. For each peak, the excitation energy in MeV is shown in the spectrum at the specific angle where it was determined. Dashed levels in level schemes are not seen or resolved in our measurements but were identified in previous experiments. The ^{22}Mg spin-parity assignments without parentheses are taken from previous experiments [35]. For highly excited states spin parities are mostly unknown. In these cases we have made assignments on the basis of comparisons with the mirror nucleus ^{22}Ne. For the ^{22}Ne levels where spin-parity values are not known experimentally we used predictions of shell-model calculations given in Ref. [36]. This was done by associating low-lying theoretical levels with experimentally measured positive-parity levels and continuing this procedure for levels with excitation energies up to 13 MeV. To emphasize that these mirror assignments of spin parities in ^{22}Mg are assumptions for the purpose of rate calculations they are shown within brackets. The shell-model excitation energies and spin parities for the $A = 22$ mirror system are presented at the right-hand sides in Figs. 8–10 and are marked by the label T. Solid arrows in the level schemes indicate the mirror assignments between ^{22}Mg and ^{22}Ne levels for which spin-parity values are already known. Dashed arrows mean that the spin parities in ^{22}Mg are not known but were assigned the values of the corresponding levels in ^{22}Ne for the purpose of this study.

A. Levels below the proton-emission threshold

In Fig. 3, spectra measured at -0.3°, 8°, and 17° are shown with the six calibration levels indicated by an asterisk. In addition to the calibration levels whose excitation energies are taken from Ref. [30], we observed two weakly excited levels at 5.2947(23) MeV and 5.454(4) MeV. We also observed at -0.3° a weakly excited state at 5.092(5) MeV that was previously observed [19,30,31,38]. The possible ^{22}Mg mirror assignments for states below the proton-emission threshold are given in Fig. 7. Table II shows an excellent agreement between our measured excitation energies and all previous results. The total errors of the excitation energies of the present ^{22}Mg level are the sums of the statistical errors due to the peak positions and a systematic error that consists of the quadratic sum due to the reaction angle errors and the systematic mass errors.

B. Levels between the proton-emission and α-emission thresholds

The high resolution of about 13 keV in the present experiment allowed us to resolve previously unresolved levels and to clarify existing ambiguities. In Fig. 4 we show three triton spectra taken at spectrometer angles of -0.3°, 8°, and 17° covering the excitation range between the proton-emission threshold at 5.5 MeV and the α-emission threshold at 8.14 MeV in ^{22}Mg. In Fig. 11, the multiplet of four states

TABLE III. Excitation energies, spins, and parities of levels in the region (5.512–8.142 MeV) between the proton-emission and α-emission thresholds.

J^{π}[a]	J^{π} Ref.	Present (p,t)	Ref. [30] (^{12}C,$2n+\gamma$)	Ref. [31] (p,t)	Ref. [19] (^{3}He,^{6}He)	Ref. [38] (^{3}He,n)	Ref. [18] (^{16}O,^{6}He)	Ref. [20] (^{4}He,^{6}He)	Ref. [39] (^{21}Na,^{22}Mg)	Ref. [40] (^{21}Na,p)	Ref. [41] (^{21}Na,p)	Adopted present[b]
2^+	[35]	5.7110[*]	5.7110(10)	5.7106(12)	5.7139	5.699(20)	5.711	–	5.7097(5)	–	–	5.7101(5)[d]
0^+[c]	[35]	5.9538(8)	–	5.9577(25)	–	5.945(20)	–	–	5.958(5)	–	–	5.9542(6)
$[3^-]$		6.0362(8)	–	6.0413(30)	6.051(4)	–	6.041(11)	6.059(9)	6.042(13)	–	–	6.0371(8)
(4^+)	[35]	6.2261(10)	–	6.2411(51)[g]	6.246(4)[g]	–	–	6.244(9)[g]	6.242(1)[g]	–	–	6.2261(10)[e]
6^+	[30]	–	6.2542(3)	6.2411(51)[g]	6.246(4)[g]	6.263(20)	6.255(10)	6.244(9)[g]	6.242(1)[g]	–	–	6.2543(3)[f]
1^+	[40]	6.306(9)	–	6.3170(60)	6.329(6)	–	–	–	6.3255(9)	6.3290(24)	–	6.3256(9)
(1^-)	[40]	6.578(7)	–	–	–	6.573(20)	–	–	–	6.587(10)	–	6.580(6)
2^+	[40]	6.602(9)	–	6.606(7)	6.616(4)	–	6.606(11)	6.606(9)	6.6053(25)	6.611(11)	6.61(15)	6.605(7)
$(1^+, 2^+)$	[41]	6.7688(12)	–	6.780(14)	6.771(5)	6.770(20)	6.767(20)	6.766(12)	–	6.792(17)	6.81(15)	6.7690(12)
$(2^+, 3^-)$	[41]	6.8760(12)	–	–	6.878(9)	–	6.889(10)	–	–	6.881	6.92(15)	6.8762(12)
$[3^+]$		7.027(9)	–	–	–	–	–	–	–	–	–	7.027(9)
$[4^+]$		7.045(7)	–	–	–	–	–	–	–	–	–	7.045(7)
$(1^+, 3^-, 2)$	[41]	7.060(7)	–	–	–	–	–	–	–	–	7.06(16)	7.060(7)
$[1^-]$		7.079(8)	–	–	–	–	–	–	–	–	–	7.079(8)
0^+	[35]	7.2183(10)	–	–	7.206(6)	7.201(20)	7.169(11)	7.216(9)	–	–	–	7.2176(9)
$[2^+]$		7.338(13)	–	–	–	–	–	–	–	–	–	7.338(13)
$(1,2^+)$	[41]	7.389(12)	–	–	7.373(9)	–	7.402(13)	–	–	–	7.42(17)	7.384(7)
$(1^+, 2^+)$	[41]	7.5995(29)	–	–	7.606(11)	–	–	7.614(9)	–	–	7.58(17)	7.6012(27)
$[2^-]$		–	–	–	–	–	7.674(18)	–	–	–	–	7.674(18)
(2^-)	[41]	7.7411(20)	–	–	7.757(11)	–	7.784(18)	–	–	–	–	7.7420(19)
(2^+)	[41]	7.9206(15)	–	–	7.916(16)	–		–	–	–	7.97(19)	7.9206(14)
$[3^-]$		8.0070(14)	–	–	7.986(16)	–	7.964(16)	7.938(9)	–	–	–	8.0051(13)
$[3^+]$		–	–	–	–	–	8.062(16)	–	–	–	–	8.062(16)

[*]Energy from Ref. [30] used for calibration in the present work.

[a]Assignments of J^{π} are from the references given in the second column. For states where no (tentative) spin assignments are known, we show in brackets spin assumptions based on the mirror assignments given in Fig. 8.

[b]Weighted average.

[c]The earlier assignment of 0^+ may have been in question due to the unresolved doublet in those studies; however, we clearly resolve this state and confirm that the 0^+ assignment is correct; for details see text.

[d]Only data from Refs. [30,38,39] are included.

[e]Only present data considered.

[f]Data included in the weighted average are from Refs. [18,30,38].

[g]Unresolved doublet.

TABLE IV. Excitation energies, spins, and parities of levels in the region (8.14–10.5 MeV) above the α-emission threshold in ^{22}Mg. Superscript T refers to theoretical values from shell-model calculations, Ref. [36].

J^π mirror	Present (p,t)	Ref. [19] [a]	Ref. [18] (^{16}O,^{6}He)	Ref. [20] (^{4}He,^{6}He)	Ref. [41] (^{21}Na,p)	Adopted present[b]
$[2^+]$	8.1803(17)	8.229(20)	8.203(23)	8.197(10)	8.17(19)	8.1812(16)
$[2^+]$	8.383(13)	8.394(21)	8.396(15)	8.380(10)	8.31(20)	8.385(7)
$[3^-]$	8.5193(21)	8.487(36)	8.547(18)[c]	8.512(10)	8.51(20)	8.5193(20)
$[4^+]^T$	8.572(6)	8.598(20)	–	–	–	8.574(6)
$[0^+]^T$	8.6575(17)	–	8.613(20)	(8.644(18))[d]	8.61(21)	8.6572(17)
$[4^+]$	8.743(14)	–	–	–	–	8.743(14)
$[1^-]$	8.7845(23)	8.789(20)	8.754(15)	8.771(9)	–	8.7832(22)
$[2^+]$	8.9331(29)	–	8.925(19)	8.921(9)	–	8.9318(27)
$[1^-]$[e]	9.082(7)	–	9.066(18)	(9.029(20))[d]	–	9.080(7)
$[4^+]^T$	9.157(4)	–	(9.172(23))	9.154(10)	–	9.157(4)
$[6^+]^T$	–	–	(9.248(20))	–	–	9.248(20)
$[2^+]^T$	9.315(14)	–	9.329(26)	(9.378(22))[d]	–	9.318(12)
$[3^-]$	9.492(13)	–	(9.452(21))		–	9.482(11)
$[2^+]$	9.546(15)	–	9.533(24)	9.542(12)	–	9.542(9)
$[6^+]^T$	–	–	9.638(21)	9.640(10)	–	9.640(9)
$[0^+]$	(9.70(5))	–	9.712(21)	–	–	9.709(19)
$[2^+]$	9.7516(27)	–	–	9.746(10)	–	9.7516(27)
$[0^+]$	9.861(6)	–	9.827(44)	9.853(11)	–	9.860(5)
$[1^+]$	–	–	9.924(28)	9.953(13)	–	9.948(12)
$[2^+]$	10.087(15)	–	10.078(24)	(10.128(20))[d]	–	10.085(13)
$[3^+]$	(10.168(9))	–	10.190(29)	–	–	10.170(8)
$[2^+]$	10.2717(17)	–	10.297(25)	10.260(10)	–	10.2715(17)
$[4^+]^T$	10.430(19)	–	10.429(26)	(10.389(20))[d]	–	10.429(13)

[a] ^{25}Mg(^{3}He,^{6}He)^{22}Mg reaction.

[b] Weighted average.

[c] Possible unresolved doublet of the levels at 8.5193(21) MeV and 8.572(6) MeV; not included in the averaging of values.

[d] The energies of these levels differ significantly from those measured in the present experiment and Ref. [18], except for the level at 8.644 MeV that has a tentative assignment in Ref. [20]; these levels are not included in the weighted average.

[e] Negative parity, in this case we assume 1^-.

between 7.027 and 7.079 MeV is shown in an expanded view of the spectrum at 8°. Possible ^{22}Ne mirror assignments for these states are shown in Fig. 8.

The ^{22}Mg excitation energies deduced from the present measurement between the proton-emission and α-emission thresholds are listed in column 3 of Table III and compared to previous experimental results.

A level measured in the energy region of 5.8–6.1 MeV was identified as 0^+ state in earlier studies on the basis of measured $L = 0$ angular distributions [38,42,43]. Chen *et al.* [18] pointed out that the large uncertainty of the deduced excitation energies suggests that there may be two unresolved levels. With a resolution of 13 keV we clearly separate two strongly excited states at 5.9538(8) and 6.0362(8) MeV that were not resolved in these earlier studies where resolutions were at best 100 keV. The strongly forward-peaked angular distributions of the earlier studies suggest that one of these two states has a spin parity of 0^+, but it is uncertain which one. The 0^+ assignment of the compilations [32,35] is, therefore, in question. We measured spectra at only three angles, but this is sufficient to determine that the angular momentum L of the state at 5.9538 MeV is $L = 0$. This can be seen from Fig. 12 and a comparison with the measured angular distribution of the ground state (g.s.) with known spin parity of 0^+. We also show the results of distorted-wave Born approximation (DWBA) calculations as dotted curves in the figure. The calculations are normalized to the measured cross sections at 0° to account for the spectroscopic factor. Details of the DWBA calculation can be found in Ref. [29]. The data as well as the DWBA calculations show that the $L = 0$ transitions have the typical strong maximum at 0° with a deep minimum around the center-of-mass scattering angle of 20° in our case. The $L = 2$ transition also has a maximum at 0°, but the minimum is less pronounced. The $L = 3$ transitions are rather flat in the measured angle range while the $L = 4$ transition has a maximum around 20°. These diffractional patterns are less pronounced in the DWBA calculations compared to the data. While the general features of the diffractional patterns of the measured and calculated angular distributions are similar, the quantitative agreement seems insufficient to allow unambiguous spin assignments. This is the reason why our 0^+ spin assignment of the 5.954-MeV state is based on the comparison with the ground state with known 0^+ spin parity. This and also the fact that there is no known low-lying 3^- state for comparison are the reasons why we cannot make a clear determination of the spin parities of the states at 6.036

TABLE V. Excitation energies, spins, and parities of levels in the region above 10.5 MeV. Superscript T indicates theoretical values from shell-model calculations, Ref. [36]. Excitation energies within parentheses indicate tentatively identified levels.

J^π mirror	Present (p,t)	Ref. [18] (^{16}O,^{6}He)	Ref. [21] (^{18}Ne,p)	Ref. [22] (^{18}Ne,p)	Ref. [20] (^{4}He,^{6}He)	Adopted present[a]
$[3^+]^T$	–	10.570(25)	(10.580(50))	10.55(14)	–	10.572(23)
$[3^-]$	10.667(19)	10.660(28)	–	10.66(14)	10.627(20)	10.651(13)
$[2^+]$	10.768(21)	10.750(31)	–	–	10.776(20)	10.768(13)
$[4^+]^T$	10.881(15)	10.844(38)	(10.820(60))	10.86(14)	–	10.873(14)
$[8^+]$	–	–	10.910(50)	10.92(14)	(10.915(20))	10.914(19)[b]
$[0^+]$	10.999(15)	10.980(31)	10.990(50)	11.01(14)	(11.015(20))	11.001(11)[b]
[6,7]	–	–	(11.050(50))	–	–	11.050(50)
$[7^-]$	–	11.135(40)	11.130(50)	–	(11.118(20))	11.122(17)[b]
$[6^+]^T$	–	–	–	–	(11.231(20))	11.231(20)[b]
$[4^+]^T$	11.317(27)	–	–	–	11.313(20)	11.315(16)
$[2^+]$	11.499(17)	–	–	–	–	11.499(17)
$[1^-]$	11.603(16)	–	–	–	11.581(20)	11.595(12)
$[0^+]$	11.76(3)	–	–	–	(11.742(20))	11.747(17)[b]
$[0^+]$	11.937(17)	–	–	–	11.881(20)	11.914(13)
$[1^-]$	–	–	–	–	(12.003(20))	12.003(20)[b]
$[3^-]$	12.220(30)	–	–	–	(12.169(20))	12.185(17)[b]
$[2^+]$	12.474(26)	–	–	–	–	12.474(26)
$[3^-]$	12.665(17)	–	–	–	–	12.665(17)
$[0^+]$	(13.01(5))	–	–	–	–	(13.01(5))

[a]Weighted average.

[b]Here we included the tentatively determined levels from Ref. [20].

and 6.226 MeV as can be seen from the figure where both states are shown together with DWBA calculations for $L = 3$ and $L = 4$. Also a comparison with the angular distribution

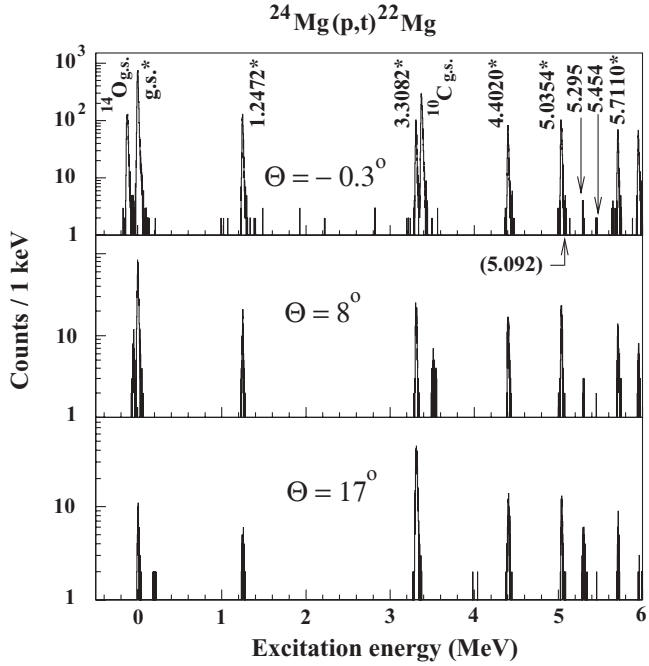

FIG. 3. These ^{24}Mg$(p,t)^{22}$Mg spectra show the low-lying states. They were taken at 98.7 MeV incident energy and at spectrometer angles $-0.3°$, $8°$, and $17°$. The calibration lines are marked by an asterisk.

of the known 4^+ state at 3.308 MeV is inconclusive. It should also be noted that a 6^+ state was reported at 6.254 MeV just 28 keV above the one at 6.226 MeV. Despite our 13-keV resolution this state is not observed in our spectra although we cannot exclude a small contribution to the peak at 6.226 MeV. During the editing process of this article a study was published by Chae *et al.* [44] claiming that they observe a 0^+ level at 6.045 MeV. This clearly contradicts our data shown in Figs. 4 and 12. Possible reasons for this discrepancy may be the fact that in the study of Chae *et al.* the resolution is not sufficient to resolve the levels at 5.954 and 6.036 MeV. They also use a single state at 6.045 MeV in their energy calibration that is in fact a doublet. Moreover, the measurement was done at center-of-mass scattering angles larger than about 20° where the differences of the $L = 0$ and $L = 3$ are less distinct compared to the forward angles. Their χ^2 is smaller for the $L = 0$ than the $L = 3$ or $L = 4$ assignment; however, it is not demonstrated that this difference is sufficient to determine the spin, e.g., by applying this method to states of well-known spins.

The assignments of earlier studies of 0^+ for the level at 5.9538 MeV may have been uncertain because this level was not resolved from the state at 6.036 MeV. However, we clearly resolve these states and can determine that the state at 5.9538 MeV has a spin parity of 0^+ as we show in Table III. For the 6.0362-MeV state as well as for those states where no previous spin-parity values are known we show spin-parity assumptions [in brackets] on the basis of the mirror assignments in Fig. 8. In Table VI where we summarize the spin parities that enter our rate calculations, we show the spin parities of both states at 5.9538 and 6.0362 MeV in brackets to

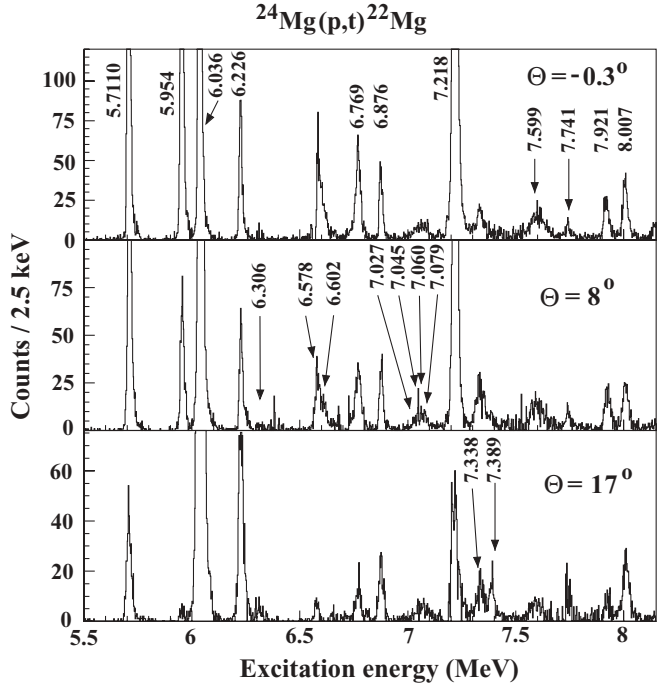

FIG. 4. The ^{22}Mg spectra measured above the proton-emission threshold. All ^{12}C$(p,t)^{10}$C and ^{16}O$(p,t)^{14}$O contaminant peaks have been subtracted. The determined excitation energies for ^{22}Mg are listed in the third column of Table III. For an expanded view of the multipet of the four states between 7.027 and 7.079 MeV, see Fig. 11.

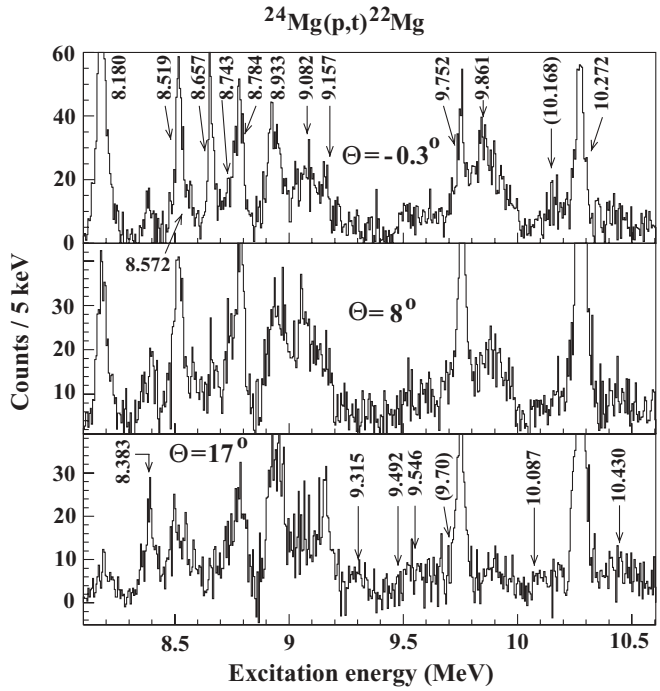

FIG. 5. The ^{22}Mg spectra above the α-emission threshold. The energy for each peak is marked in the specific spectrum, where it was determined at $-0.3°$, $8°$, or $17°$. All ^{12}C$(p,t)^{10}$C and ^{16}O$(p,t)^{14}$O contaminant peaks were subtracted. The excitation energies determined for ^{22}Mg are listed in the second column of Table IV.

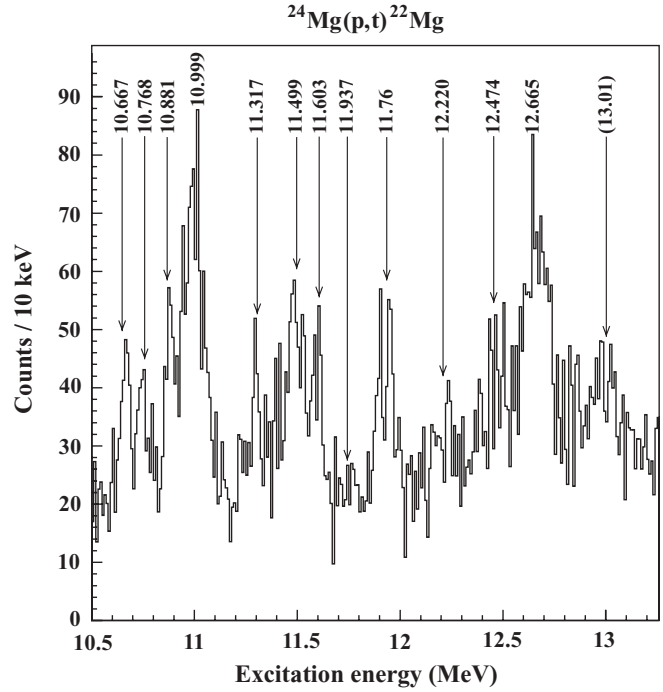

FIG. 6. The ^{24}Mg$(p,t)^{22}$Mg spectrum above 10.5 MeV, measured at the scattering angle of 17°. The excitation energies determined for ^{22}Mg are listed in the second column of Table V.

indicate that these are assumptions, namely $[0^+]$ for the former and $[3^-]$ for the latter state.

Bateman *et al.* [31] measured a peak at 6.241 MeV (see Table I) with a relatively large width of 26 ± 6 keV. They suggested that it consisted of a doublet. This conjecture was confirmed by Seweryniak *et al.* [30] when they resolved the doublet by measuring a 6^+ state at 6.254 MeV. In the present (p,t) experiment we observed only one level at the lower excitation energy of 6.2261(10) MeV with a width of 13 keV corresponding to the energy resolution of the present experiment. This level probably corresponds to the ^{22}Ne 4^+ state at 6.346 MeV.

We confirmed the existence of a doublet at 6.587(10) MeV and 6.611(11) MeV resolved by Ref. [40] by measuring levels at 6.578(7) MeV and 6.602(9) MeV. Due to our high resolution, we resolved four closely spaced levels at 7.027(9) MeV, 7.045(7) MeV, 7.060(7) MeV, and 7.079(8) MeV for the first time. These four levels are probably the analog states to the closely spaced levels above 7.343 MeV in ^{22}Ne. In addition, we observed new states at 7.338(13) MeV and 7.9206(15) MeV.

A recent proton scattering experiment by He *et al.* [41] used inverse kinematics ^{1}H$(^{21}$Na$,p)^{21}$Na with a radioactive ^{21}Na beam to provide additional information in this excitation range in ^{22}Mg. Their R-matrix analysis identified a number of levels at the same excitation energies were we also see levels within the experimental uncertainties. However, the spin and parity assignments of He *et al.* [41] are not unique as can be seen from Table III. Our spin-parity assumptions, shown in Table VI, based on mirror assignments are consistent with their values except for the states at 6.876 and 7.389 MeV.

TABLE VI. Summary of levels included in the calculations of the reactions rates with theoretically and experimentally obtained S_α values of ^{22}Ne for states with spins smaller than 5 (ground state = g.s.). Superscript T indicates theoretical value from shell-model calculations, Ref. [36].

E_x (^{22}Mg) adopted –	J^π adopted –	E_x (^{22}Ne) Ref. [35] –	E_x (^{22}Ne) SACM model	S_α SACM model	S_α[a] Ref. [45] ^{18}O(^{6}Li,d)	S$_\alpha$[b] Ref. [46] ^{18}O(^{7}Li,t)	S_α[c] Ref. [47] ^{18}O(^{6}Li,d)	S_α – ^{18}O(α,γ)	Average S_α – –
g.s.	0^+	g.s.	g.s.	0.067	0.067	0.079	–	–	0.071
1.24718(3)	2^+	1.275	1.275	0.051	0.021	0.018	–	–	0.030
3.30821(6)	4^+	3.358	4.250	0.024	0.007	–	–	–	0.016
4.4020(29)	2^+	4.456	4.455	0.000	0.006	–	–	–	0.003
5.0346(5)	2^+	5.363	5.622	0.026	0.002	–	–	–	0.014
5.2938(10)	4^+	5.524	7.430	0.004	0.002	–	–	–	0.003
5.7101(5)	2^+	6.120	–	–	–	–	–	–	–
5.9542(6)	$[0^+]$	6.234	6.216	0.124	0.058	0.354	–	–	0.179
6.0371(8)	$[3^-]$	5.910	6.897	0.024	0.002	0.043	–	–	0.023
6.2261(10)	$[4^+]$	6.347	–	–	0.004	–	–	–	0.004
6.580(6)	$[1^-]$	6.691	4.772	0.067	–	0.213	–	–	0.140
6.605(7)	2^+	6.819	6.810	0.011	–	0.085	–	–	0.048
6.7690(12)	$[1^+]$	6.900	–	–	–	–	–	–	–
6.8762(12)	$[1^-]$	7.051	5.960	0.011	–	0.170	–	–	0.091
7.045(7)	$[4^+]$	7.343	–	–	–	–	–	–	–
7.060(7)	$[3^-]$	7.406	–	–	–	0.028	–	–	0.028
7.079(8)	$[1^-]$	7.491	–	–	–	0.213	–	–	0.213
7.2176(9)	0^+	7.341	7.408	0.510	0.050	0.510	–	–	0.357
7.338(13)	$[2^+]$	7.643	7.491	0.108	0.020	–	–	–	0.064
7.384(7)	$[3^-]$	7.722	–	–	–	–	–	–	–
7.6012(27)	$[2^+]$	7.923	–	–	–	0.028	–	–	0.028
7.7420(19)	$[4^+]$	8.076	8.597	0.065	–	–	–	–	0.065
7.9206(14)	$[2^+]$	8.134	8.683	0.476	–	0.368	–	–	0.422
8.0051(13)	$[3^-]$	8.376	8.085	0.060	–	0.028	–	–	0.044
8.1812(16)	$[2^+]$	8.489	–	–	–	0.567	0.001	–	0.284
8.385(7)	$[2^+]$	8.596	–	–	–	0.567	0.082	–	0.325
8.5193(20)	$[3^-]$	8.740	–	–	–	–	0.004	–	0.004
8.574(6)	$[4^+]^T$	8.855	9.785	0.060	–	–	–	–	0.060
8.6572(17)	$[0^+]^T$	8.899	–	–	–	–	–	–	–
8.743(14)	$[4^+]$	8.976	–	–	–	–	0.022	–	0.022
8.7832(22)	$[1^-]$	9.097	–	–	–	–	–	–	–
8.9318(27)	$[2^+]$	9.229	–	–	–	–	–	–	–
9.080(7)	$[1^-]^T$	9.324	–	–	–	–	–	–	–
9.157(4)	$[4^+]^T$	9.508	10.466	0.078	–	–	–	–	0.078
9.318(12)	$[2^+]^T$	9.625	–	–	–	–	–	–	–
9.482(11)	$[3^-]$	9.725	–	–	–	–	0.018	0.011[d]	0.015
9.542(9)	$[2^+]$	9.842	–	–	–	–	0.029	0.027[d]	0.028
9.709(19)	$[0^+]$	10.066	–	–	–	–	0.145	0.150[d]	0.148
9.7516(27)	$[2^+]$	10.137	–	–	–	–	–	0.019[d]	0.019
9.860(5)	$[0^+]$	10.283	–	–	–	–	–	0.019[e]	0.019
10.085(13)	$[2^+]$	10.297	–	–	–	–	–	0.050[e]	0.050
10.2715(17)	2^+	10.551	–	–	–	–	–		–
10.429(13)	$[4^+]^T$	10.749	–	–	–	–	–		–
10.651(13)	$[3^-]$	10.857	–	–	–	–	–	3.0×10^{-5}[f]	3.0×10^{-5}
10.768(13)	$[2^+]$	11.064	–	–	–	–	–		–
10.873(14)	$[0^+]^T$	11.194	–	–	–	–	–	1.0×10^{-6}[f]	1.0×10^{-6}
11.001(11)	$[4^+]^T$	11.271	–	–	–	–	–	2.0×10^{-5}[f]	2.0×10^{-5}
11.315(16)	$[4^+]^T$	11.577	–	–	–	–	–		–
11.499(17)	$[2^+]$	11.708	–	–	–	–	–	–	–
11.595(12)	$[1^-]$	11.896	14.844	0.054	–	–	–	–	0.054
11.747(17)	$[0^+]$	12.071	–	–	–	–	–	–	–
11.914(13)	$[0^+]$	12.218	–	–	–	–	–	–	–
12.003(20)	$[1^-]$	12.280	–	–	–	–	–	0.207[g]	0.207

TABLE VI. (*Continued.*)

E_x (^{22}Mg) adopted –	J^π adopted –	E_x (^{22}Ne) Ref. [35] –	E_x (^{22}Ne) SACM model	S_α SACM model	S_α[a] Ref. [45] ^{18}O(^{6}Li,d)	S_α[b] Ref. [46] ^{18}O(^{7}Li,t)	S_α[c] Ref. [47] ^{18}O(^{6}Li,d)	S_α – ^{18}O(α,γ)	Average S_α – –
12.185(17)	[3$^-$]	12.390	12.969	0.150	–	–	–	0.210[g]	0.180
12.474(26)	[2$^+$]	12.643	–	–	–	–	–	–	–
12.665(17)	[3$^-$]	12.862	–	–	–	–	–	0.120[g]	0.120
(13.010(50))	[0$^+$]^T	13.274	–	–	–	–	–	–	–

[a]Normalized to g.s. 0$^+$ calculated in the SACM model.
[b]Normalized to 7.341 MeV 0$^+$ calculated in the SACM model.
[c]Normalized on 10.066 MeV 0$^+$ from Ref. [48].
[d]S_α factors taken from Ref. [48].
[e]S_α factors taken from Ref. [49].
[f]S_α factors taken from Ref. [50].
[g]S_α factors taken from Ref. [37].

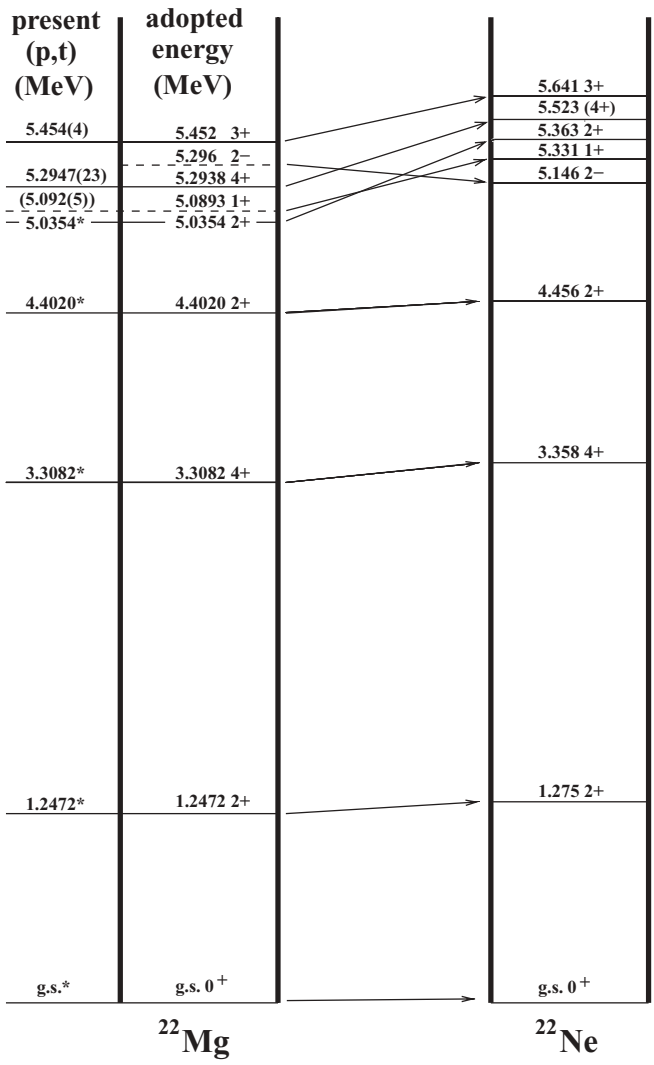

FIG. 7. The ^{22}Mg mirror assignments for states below the proton-emission threshold are shown. The ^{22}Mg spin-parity assignments are taken from previous experiments [30,35] as shown in detail in Table II. The spin-parity values of the mirror nucleus ^{22}Ne are taken from Ref. [35].

C. Levels above the α-emission threshold

We will first discuss levels between the α-emission threshold and 10.5 MeV and then levels above 10.5 MeV.

1. *Levels between the α-emission threshold and 10.5 MeV*

The ^{22}Mg levels above the α-emission threshold are important for the ^{18}Ne$(\alpha,p)^{21}$Na reaction above 0.8 GK. The triton spectra measured at spectrometer angles -0.3°, 8°, and 17° in the excitation-energy range between 8.14 and 10.5 MeV are shown Fig. 5. The mirror spin-parity assignments that we used for the ^{22}Mg levels in this excitation-energy range are shown in Fig. 9. Because of the lack of positive-parity levels in Ref. [36] the 9.324-MeV level in ^{22}Ne is assigned to have 1^- spin parity. The excitation energies given in parentheses are tentative. These spin-parity assignments shown for the adopted levels were used in reaction-rate calculations. Table IV shows the present results together with the results from previous experiments [18–20,41]. The last column lists the level energies that were used in the reaction-rate calculations.

The level at 8.1803(17) MeV is the first level above the α-emission threshold. The excitation energy is in agreement with the energy in Ref. [18] but in disagreement with Refs. [19,20]. Due to our high-resolution spectra we were able to identify five levels at 8.5193(21) MeV, 8.572(6) MeV, 8.6575(17) MeV, 8.743(14) MeV, and 8.7845(23) MeV, where the level at 8.743(14) MeV was resolved for the first time. The excitation energies for these five levels were deduced from the measurement at -0.3° (see Fig. 13). All observed levels are shown in Fig. 9. In this excitation-energy region of ^{22}Mg, the present uncertainties in the excitation energies are improved by up to a factor of 5 as compared to previous results. Because the excitation energies of resonance levels enter exponentially in the rate calculations, the uncertainties originating from these errors are greatly reduced.

2. *Levels above 10.5 MeV*

The ^{22}Mg levels in the region above 10.5 MeV are important for x-ray bursts and supernovae at peak temperatures around 2.5 GK. Previous studies [18,20–22] succeeded in identifying

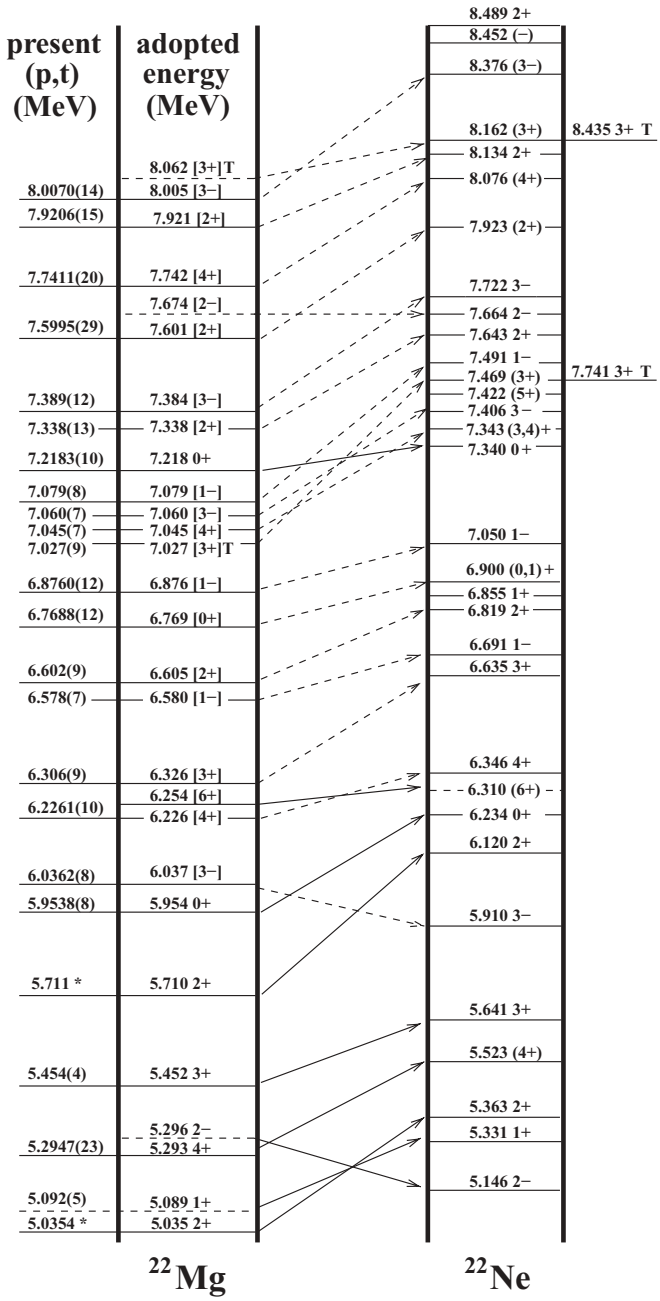

FIG. 8. The ^{22}Mg mirror assignments for states between 5 MeV and the α-emission threshold at 8.140 MeV. For details, see text.

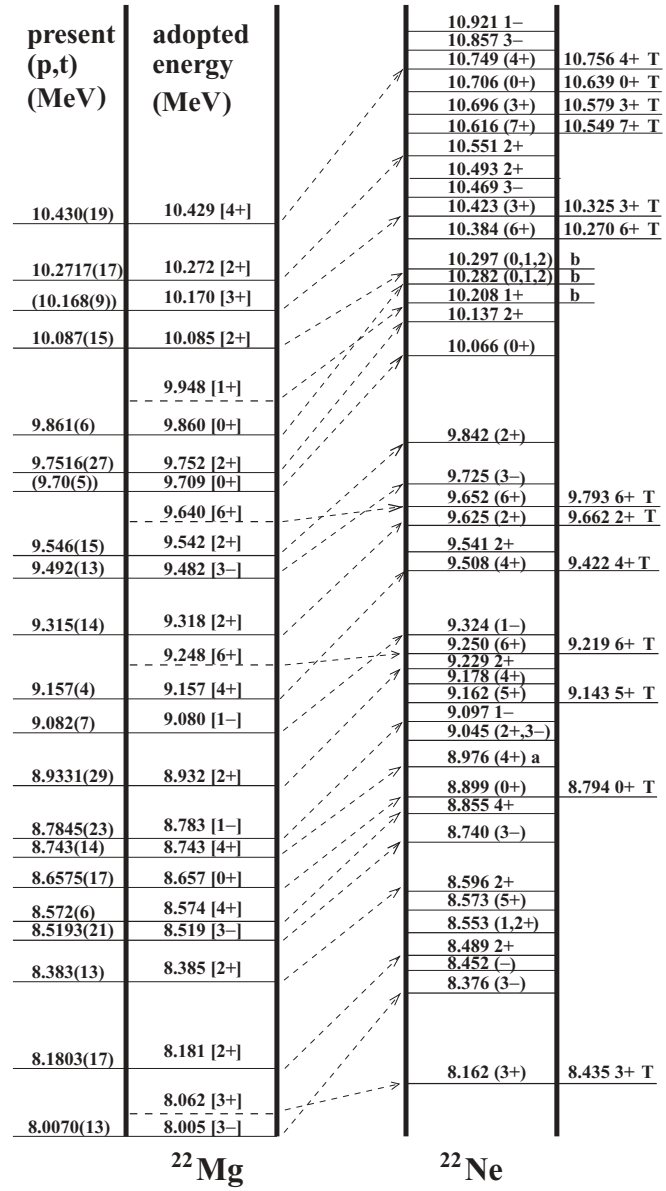

FIG. 9. Mirror spin-parity assignments for the ^{22}Mg levels above the α-emission threshold. The excitation-energy and spin-parity values marked by the superscript T are from shell-model calculations, Ref. [36]. Level energies for ^{22}Ne were taken from Ref. [35]. The spin-parity value labeled a is from Ref. [13]. The excitation energies labeled b are from Ref. [32].

several levels in this region. The resolution achieved in previous experiments was, however, insufficient to resolve most states. We have measured spectra at scattering angles of 8° and 17° for this excitation-energy region. Due to the lower statistics and larger uncertainties in the scattering angles errors of 5 and 10 keV were added to the errors of the excitation energies for the 8° and 17° results, respectively. Because of the larger number of counts collected at the spectrometer angle of 17°, we adopted the ^{22}Mg excitation energies determined from this spectrum. Figure 6 presents the spectrum taken at 17° where all impurity lines were subtracted. A level was adopted if identified at both angles. The spin-parity assignments that we used for the ^{22}Mg levels are shown in Fig. 10. Our results, together with the data from previous experiments, are summarized in Table V. In the last column of Table V, we list the averaged excitation energies from all experiments, including the tentatively identified peaks from Ref. [20]. We confirmed the existence of the level at 11.742(20) MeV that was tentatively identified in Ref. [20].

V. STELLAR REACTION RATES

Because of the high level density in ^{22}Mg above the α threshold, many resonances contribute to the reaction rate.

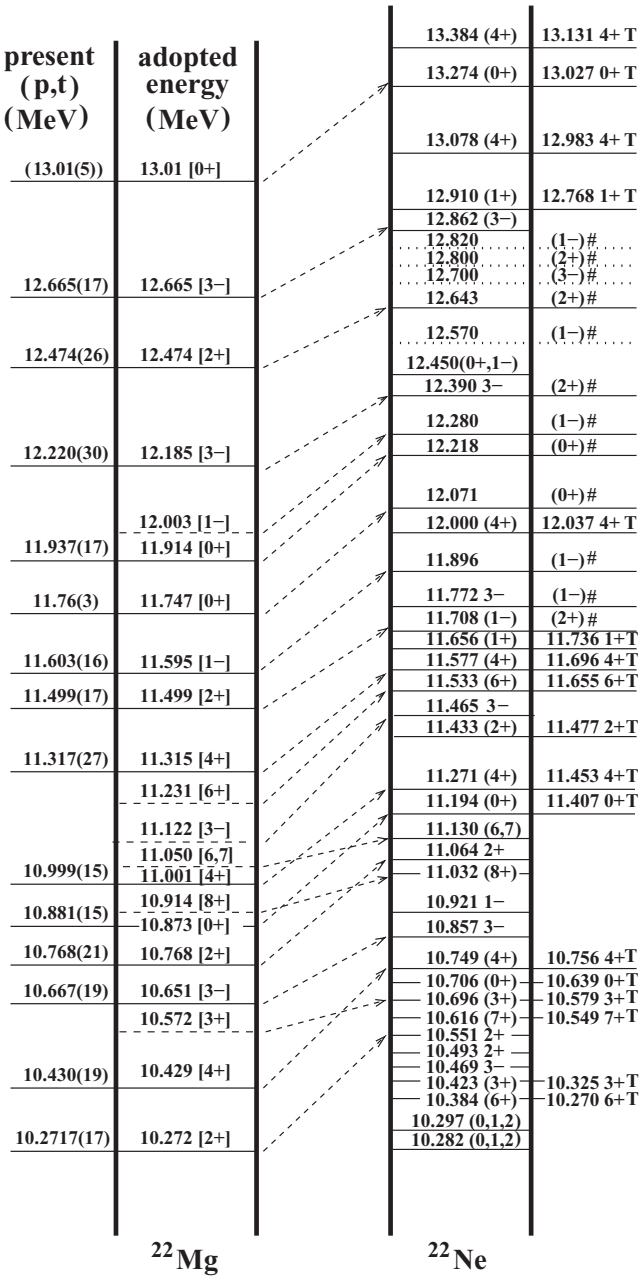

FIG. 10. Spin-parity assignments for the ^{22}Mg levels above 10.5 MeV. Assignments marked by a # were taken from Ref. [37]. For further details, see text.

Tail contributions can therefore be neglected and we adopted the narrow resonance formalism [51] to calculate the reaction rate. Within the framework of this formalism, the total reaction rate, $N_A\langle\sigma\upsilon\rangle$, can be expressed as the sum over individual resonances i:

$$N_A\langle\sigma\upsilon\rangle = 1.54\times10^{11}(\mu T_9)^{-3/2}\sum_i(\omega\gamma)_i \times\exp(-11.605E_i/T_9)[\mathrm{cm}^3\ \mathrm{s}^{-1}\ \mathrm{mol}^{-1}] \quad (3)$$

with μ the reduced mass of the target and projectile in units of amu, T_9 the temperature in units of GK, and $(\omega\gamma)_i$ and E_i the strength and energy of the ith resonance in units of MeV, respectively.

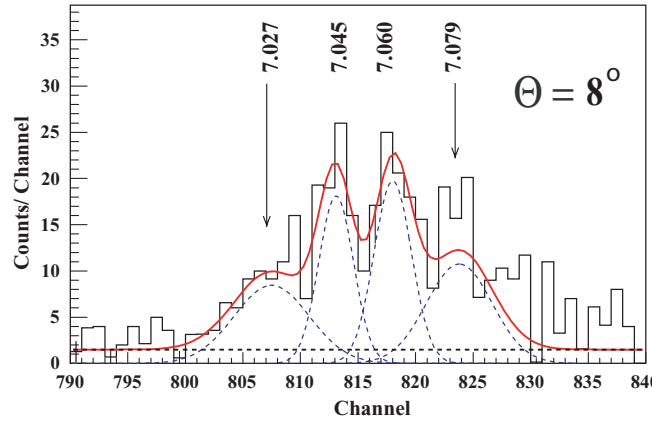

FIG. 11. (Color online) Expanded view of the multiplet of four states between 7.027 and 7.079 MeV in the ^{22}Mg spectra shown in Fig. 4. The fitted curve (solid line) consists of the the sum of four Gaussian peaks and a constant background (dashed lines).

It can be seen from Eq. (3) that because of the exponential dependence, the largest uncertainties in the reaction-rate calculations are introduced by errors in the resonance energy. In previous calculations, the uncertainty in the resonance energies represents the dominant uncertainty in the reaction rates. However, the high accuracy of the present measurement reduces this error significantly so that the remaining errors in the ^{21}Na$(\alpha,p)^{21}$Ne rate calculations are mainly due to the uncertainties in the resonance strengths $\omega\gamma$.

Measured resonance strengths [21,22] were previously reported for seven and eight levels, respectively. They differ by

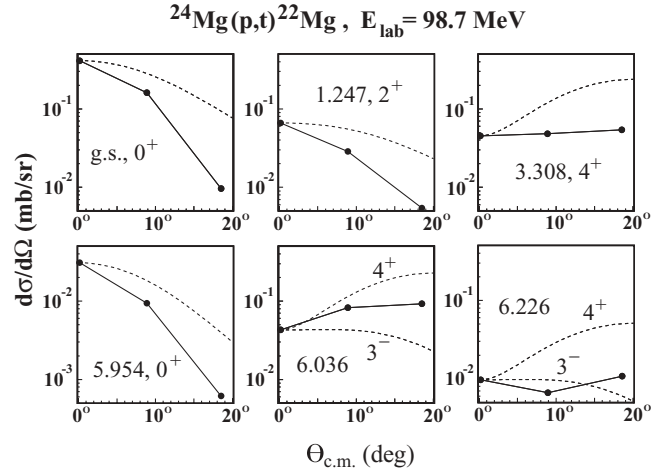

FIG. 12. Shown are cross-section angular distributions of six states in ^{22}Mg labeled by their excitation energies in units of MeV. The measured data points at three angles are connected by solid lines to guide the eye. Statistical errors are smaller than the data points. The dotted curves represent DWBA calculations. The spin parities of the three states in the upper panels are well known. For a discussion of the spin parities of the group of three states around 6 MeV; see text.

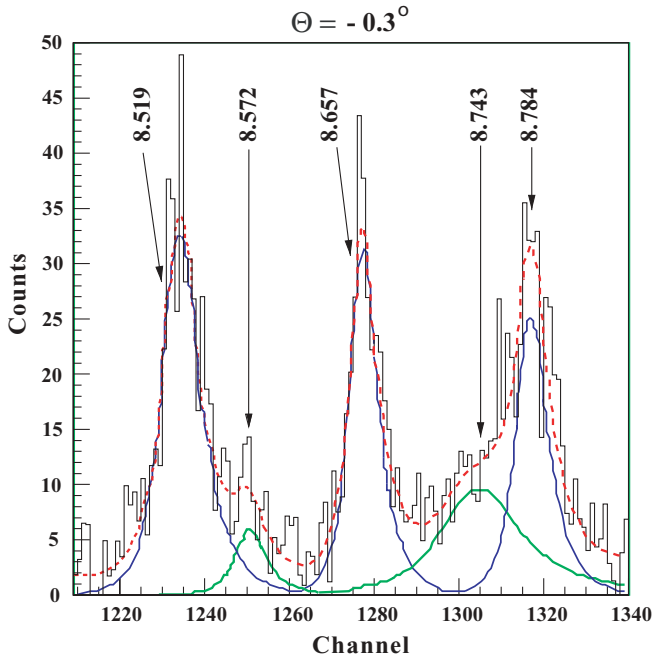

FIG. 13. (Color online) Spectrum of the ^{24}Mg$(p,t)^{22}$Mg reaction taken at an angle of -0.3° with fits to the five resolved levels between 8.5 and 8.8 MeV. The dashed line is the sum of the individual peaks shown as solid lines and a constant background of two counts. The excitation energies determined for ^{22}Mg are listed in the second column of Table IV.

up to an order of magnitude. Groombridge *et al.* [22] resolved eight ^{22}Mg levels with energies in good agreement with our adopted values. The only exception is the first level that may be an unresolved doublet that we observe at 10.087 and 10.168 MeV. We used the resonance strengths of Groombridge except for the unresolved doublet.

In the case of narrow resonances, the strengths for a reaction $a + B \longrightarrow c + D$ can be calculated by:

$$\omega\gamma = \omega\frac{\Gamma_a\Gamma_c}{\Gamma} = \frac{2J+1}{(2J_a+1)(2J_B+1)}(1+\delta_{aB})\frac{\Gamma_a\Gamma_c}{\Gamma}, \quad (4)$$

(see Ref. [51]). The particle partial widths can be calculated as:

$$\Gamma_{\text{part}} = \frac{3\hbar^2}{\mu R_n^2} P_l C^2 S_{\text{part}}, \quad (5)$$

where μ is the reduced mass of the interacting particles, S_{part} is the spectroscopic factor (in our case of protons or α particles), C is the Clebsch-Gordan coefficient, and P_l is the penetrability through the Coulomb barrier and centrifugal barrier for the orbital momentum l evaluated at an interaction radius R_n.

Our rate calculation depends critically on the spectroscopic factors S_α of the observed states. These parameters are not known experimentally. Therefore, we assign levels in ^{22}Mg to their mirror levels in ^{22}Ne to adopt the corresponding α-spectroscopic factors that were obtained through ^{18}O(^{6}Li,d) α-transfer measurements [48], ^{18}O(α,γ) α-capture studies [49,50], and ^{18}O(α,α)-scattering measurements [37]. Where no data is available, we adopted theoretical estimates based on α-cluster calculations for $A = 22$ nuclei.

The calculation of the spectroscopic factor is based on the SACM. Within this model the Hilbert space is microscopic, i.e., the Pauli exclusion principle is satisfied. The Hamiltonian, however, is phenomenological and for the case when one cluster is spherical it is of the form as given in Ref. [25] Eq. (5.4)]. The SACM has been applied with great success to many light nuclear systems [52–58], which raises the confidence that this model can describe approximately light nuclear systems.

For the system discussed in this article, the parameters were adjusted such that the spectrum at low excitation energy is reproduced. With these adjusted parameters, the density of states at high excitation energies should be described well. The expression for the algebraic parametrizations of the spectroscopic factor is given in Ref. [59]. There, the operator of the spectroscopic factor is divided into two factors. One is proportional to the square of SU(3) isoscalar factors [60], representing the dependence on the SU(3) coupling. The second factor is an exponential term with a linear combination of operators in its argument like the number of relative oscillations, the second order SU(3) Casimir operator of the clusters, the coupling of them, and the total second order SU(3) Casimir operator. Applied to the SU(3) basis, assumed to be approximately realized, these operators give simple numbers [59]. Because the construction of the model space is easy to perform, the expression of the spectroscopic factor is analytic. There are in total eight parameters, which were fitted to five different cluster systems, corresponding to nuclei in the *sd* shell. In total 17 states have been adjusted and the spectroscopic factors of 89 systems were calculated, most of them with one α cluster. The agreement with microscopic SU(3) calculations [61,62] is excellent (consult the Tables in Ref. [59]). In the present study, we did not change these parameters at all, i.e., the calculation can be considered as parameter free, although an additional fitting would surely improve the agreement to experimental data.

The S_α values adopted for each state are summarized in Table VI. For the levels where no S_α values are known, neither theoretically nor experimentally, we adopted an average S_α-spectroscopic factor that was calculated as the average of the known S_α values with the same J^π. The adopted "constant values" are $S_\alpha(0^+) = 0.11$, $S_\alpha(1^-) = 0.11$, $S_\alpha(2^+) = 0.11$, $S_\alpha(3^-) = 0.05$, and $S_\alpha(4^+) = 0.03$. Thus, all levels with a J^π of 0^+ and an unknown S_α value were assigned an S_α value of 0.11 and so on for the levels with other spin assignments. Using averaged spectroscopic factors for the unknown S_α values in our calculations will allow an easier comparison and improvement once more accurate data become available.

Parameters used in the present ^{18}Ne$(\alpha,p)^{21}$Na reaction-rate calculations are listed in Table VII. The mirror spin assignments given in Tables IV and V and in Figs. 9 and 10 are used in our calculations of the reaction rates because these spin assignments allow us to use the known S_α values of ^{22}Ne.

TABLE VII. The spin values and resonance strengths of the levels at center-of-mass energies E_{res} (c.m.) used in the calculations of the rates for the ^{18}Ne$(\alpha,p)^{21}$Na reaction.

E_x (MeV)	E_{res} (c.m.) (MeV)	J^{π}[a]	S_α	Γ_α (eV)	$\omega\gamma$ (eV)
8.1812(16)	0.039	$[2^+]$	2.8×10^{-1}	1.7×10^{-65}	8.53×10^{-65}
8.385(7)	0.243	$[2^+]$	3.2×10^{-1}	2.7×10^{-18}	1.33×10^{-17}
8.5193(20)	0.377	$[3^-]$	4.0×10^{-3}	7.0×10^{-15}	4.87×10^{-14}
8.574(6)	0.432	$[4^+]$	6.0×10^{-2}	3.6×10^{-13}	3.26×10^{-12}
8.6572(17)	0.515	$[0^+]$	1.1×10^{-1}[b]	5.0×10^{-8}	4.97×10^{-8}
8.743(14)	0.601	$[4^+]$	2.2×10^{-2}	5.7×10^{-10}	5.15×10^{-9}
8.7832(22)	0.642	$[1^-]$	1.1×10^{-1}[b]	4.0×10^{-6}	1.21×10^{-5}
8.9318(27)	0.790	$[2^+]$	1.1×10^{-1}[b]	8.3×10^{-5}	4.13×10^{-4}
9.080(7)	0.938	$[1^-]$	1.1×10^{-1}[b]	7.7×10^{-3}	2.31×10^{-2}
9.157(4)	1.015	$[4^+]$	7.8×10^{-2}	9.7×10^{-5}	8.70×10^{-4}
9.318(12)	1.176	$[2^+]$	1.1×10^{-1}[b]	9.9×10^{-2}	4.97×10^{-1}
9.482(11)	1.342	$[3^-]$	1.5×10^{-2}	1.8×10^{-2}	1.25×10^{-1}
9.542(9)	1.401	$[2^+]$	2.8×10^{-2}	3.6×10^{-1}	1.78
9.709(19)	1.565	$[0^+]$	1.5×10^{-1}	5.2×10^{1}	5.18×10^{1}
9.7516(27)	1.610	$[2^+]$	1.9×10^{-2}	1.6	8.22
9.860(5)	1.718	$[0^+]$	1.9×10^{-2}	2.1×10^{1}	2.07×10^{1}
10.085(13)	1.944	$[2^+]$	5.0×10^{-2}	4.5×10^{1}	2.25×10^{2}
10.2715(17)	2.130	2^+	–[c]	–[c]	1.03×10^{4}[c]
10.429(13)	2.287	$[4^+]$	–[c]	–[c]	7.30×10^{3}[c]
10.651(13)	2.513	$[3^-]$	–[c]	–[c]	1.82×10^{4}[c]
10.768(13)	2.626	$[2^+]$	1.1×10^{-1}[b]	2.3×10^{3}	1.16×10^{4}
10.873(14)	2.734	$[0^+]$	–[c]	–[c]	4.52×10^{4}[c]
11.001(11)	2.859	$[4^+]$	–[c]	–[c]	8.10×10^{3}[c]
11.315(16)	3.173	$[4^+]$	3.0×10^{-2}[b]	2.0×10^{2}	1.83×10^{3}
11.499(17)	3.357	$[2^+]$	1.1×10^{-1}[b]	1.7×10^{4}	8.64×10^{4}
11.595(12)	3.455	$[1^-]$	5.4×10^{-2}	2.0×10^{4}	6.11×10^{4}
11.747(17)	3.607	$[0^+]$	1.1×10^{-1}[b]	7.1×10^{4}	7.13×10^{4}
11.914(13)	3.780	$[0^+]$	1.1×10^{-1}[b]	8.8×10^{4}	8.82×10^{4}
12.003(20)	3.861	$[1^-]$	2.1×10^{-1}	1.4×10^{5}	4.31×10^{5}
12.185(17)	4.050	$[3^-]$	1.8×10^{-1}	3.7×10^{4}	2.60×10^{5}
12.474(26)	4.332	$[2^+]$	1.1×10^{-1}[b]	7.8×10^{4}	3.89×10^{5}
12.665(17)	4.523	$[3^-]$	1.2×10^{-1}	4.9×10^{4}	3.45×10^{5}
(13.010(50))	4.865	$[0^+]$	1.1×10^{-1}[b]	2.2×10^{5}	2.16×10^{5}

[a]Spin for the mirror assignments given in Figs. 9 and 10.
[b]Constant S_α values as explained in the text.
[c]Resonance strengths are measured in Ref. [22].

Calculated reaction rates for the astrophysically interesting range of temperatures are summarized in Table VIII. These rates are also shown in Fig. 14 and compared with previous calculations [13,18,21,22]. The curve labeled HF is a Hauser Feshbach calculation taken from Ref. [13]. In the temperature range from 0.3 GK to about 1 GK the HF calculation of the ^{18}Ne$(\alpha,p)^{21}$Na reaction rate is larger than any other previous prediction but is still about a factor of 5 smaller than our calculation. At 0.3 GK this enhancement is the result of mainly two levels at center-of-mass resonance energies of $E_{res} = 0.515$ and 0.642 MeV with spin-parities of $[0^+]$ and $[1^-]$, respectively. At a higher temperature of 0.4 GK mainly three levels contribute to the reaction rates. These are the levels at $E_{res} = 0.642$, 0.790, and 0.934 MeV with assumed spin-parities of $[1^-]$, $[2^+]$, and $[1^-]$, respectively. In Fig. 14, note that the reaction-rate calculation of Groombridge *et al.* [22] has a similar shape as the present calculation for temperatures above 1 GK. The reason for the shape similarity between our calculations and those of Refs. [13,18,21,22] are that we adopted the S_α values taken from those references [13,37]. The first-excited level above the α-emission threshold does not contribute significantly to the reaction rates because it is below the Gamow window for the ^{18}Ne$(\alpha,p)^{21}$Na reaction at the predicted x-ray burst temperatures.

Because the spin assignments in the present calculations are to some extent arbitrary, we checked the influence of the spin assignments by comparing our mirror assignments with a randomly generated spin distribution. The upper limit for a randomly generated spin was 6. This number was chosen because the ratio of the penetrabilities for states having spin 0 and 6 can be as large as 10,000. Furthermore, equal probability for all possible spins is assumed. The second restriction was to preserve the S_α values that we adopted from Refs. [13,37]. Thus, we assumed that the corresponding levels have a properly determined spin and S_α values. The difference between the various predictions for the total ^{18}Ne$(\alpha,p)^{21}$Na

TABLE VIII. Calculated rates of the ^{18}Ne$(p,\alpha)^{20}$Na reaction as a function of temperature.

Temperature (10^9 K)	$N_A\langle\sigma v\rangle$ (cm^3 mole^{-1} s^{-1})
0.10	5.98×10^{-24}
0.15	1.60×10^{-19}
0.20	1.78×10^{-15}
0.25	7.40×10^{-13}
0.30	5.42×10^{-11}
0.40	2.05×10^{-8}
0.50	1.32×10^{-6}
0.60	2.97×10^{-5}
0.80	2.37×10^{-3}
1.00	5.93×10^{-2}
1.5	$2.15 \times 10^{+1}$
2.0	$8.01 \times 10^{+2}$
2.5	$7.87 \times 10^{+3}$
3.0	$3.78 \times 10^{+4}$
4.0	$2.96 \times 10^{+5}$
5.0	$1.11 \times 10^{+6}$
6.0	$2.82 \times 10^{+6}$
8.0	$9.26 \times 10^{+6}$
10.0	$1.86 \times 10^{+7}$

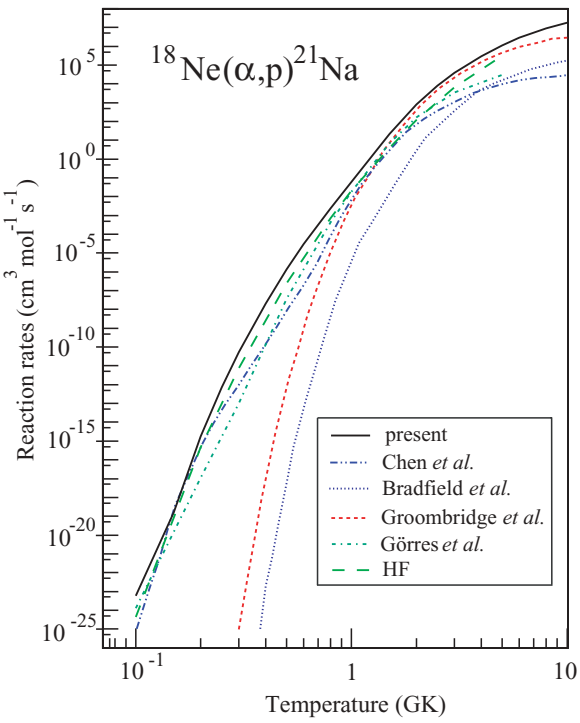

FIG. 14. (Color online) The ^{18}Ne$(\alpha,p)^{21}$Na reaction rates calculated as a function of temperature. The different curves indicate reaction rates calculated by Chen *et al.* [18], Bradfield *et al.* [21], Groombridge *et al.* [22], Görres *et al.* [13], as well as the one calculated in the present work with S_α values from those references.

reaction rates, based on randomly produced spin values and on assigned mirror spin values, was found to be within an order of magnitude.

VI. ASTROPHYSICAL IMPLICATIONS

As outlined in the Introduction, the hot CNO cycle, ^{12}C(p,γ) ^{13}N(p,γ) ^{14}O$(\beta^+\nu)^{14}$N$(p,\gamma)^{15}$O$(\beta^+\nu)^{15}$N$(p,\alpha)^{12}$C, converts hydrogen into helium. This eventually becomes unstable and sets up the conditions for the thermonuclear runaway and the resulting x-ray burst during the accretion phase. Another important cycle during the accretion phase that also converts hydrogen into helium is ^{15}O(α,γ) ^{19}Ne$(\beta^+\nu)$ ^{19}F(p,α) ^{16}O(p,γ) ^{17}F(p,γ) ^{18}Ne$(\beta^+\nu)$ ^{18}F$(p,\alpha)^{15}$O, where ^{19}Ne(p,γ) ^{20}Na provides a breakout into the *rp* process [11]. Once the atmosphere in the ignition region heats sufficiently, a second cycle starts, ^{14}O(α,p) ^{17}F(p,γ) ^{18}Ne$(\beta^+\nu)$ ^{18}F$(p,\alpha)^{15}$O [11]. The breakout from this cycle, ^{18}Ne$(\alpha,p)^{21}$Na, starts the *αp* process, which, unlike the *rp* process, is not subject to temperature-independent β^+ decays.

After the runaway starts, the ^{14}O$(\alpha,p)^{17}$F reaction flow rises from 1/3 of the ^{15}O$(\alpha,\gamma)^{19}$Ne reaction flow to over 5 times that within 1.5–2 s. Because both ^{14}O$(\alpha,p)^{17}$F and ^{17}F$(p,\gamma)^{18}$Ne are several orders of magnitude faster than ^{18}Ne$(\alpha,p)^{21}$Na, the ^{18}Ne(α,p) ^{21}Na reaction rate determines the feed to the *αp* process during the 1.5–2 s window mentioned above. Because we showed that the rate is stronger than the previously published rate in the temperature range of 0.4–0.8 GK, we conclude that the *αp* process burns faster than previously thought resulting in a faster rise in temperature and burning rapidly helium.

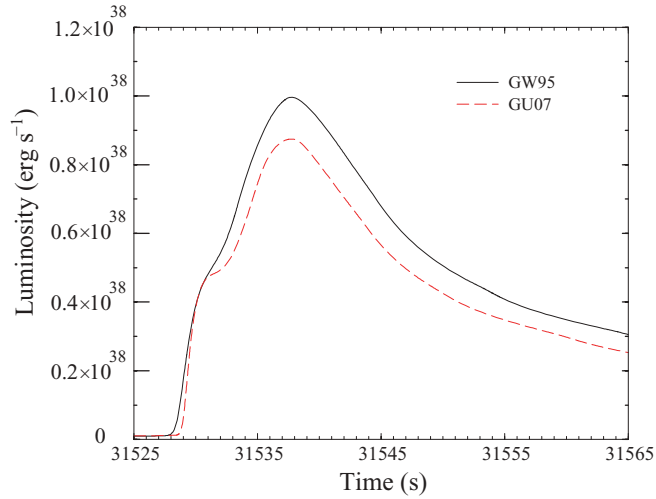

FIG. 15. (Color online) The two luminosity curves have been calculated on the basis of the previously published reaction rate (GW95) [13] and the present rate (GU07). The difference between the two curves demonstrates the impact of the modified ^{18}Ne$(\alpha,p)^{21}$Na reaction rate on the light curve of a type I x-ray burst calculated in the framework of a spherically symmetric model [9,11].

We have performed x-ray burst simulations using a multi-mass zone spherically symmetric model [9,11] to investigate the impact of this change in reaction rate. We performed this analysis by comparing the present rate with the substantially lower rate predicted by Görres *et al.* [13]. Figure 15 shows the light curve corresponding to the use for the previous rates (GW95) [13] and the present rate (GU07). The use of the new rate translates into an initially slightly sharper rise in the luminosity until the first waiting point of the αp process is reached. The reaction flow is delayed at the sequence of waiting points, ^{22}Mg, ^{26}Si, ^{30}S, and ^{34}Ar, causing lower peak luminosities as the reaction flow subsequently decays from the waiting point with less fuel available for continued rp-process burning [63]. A sharper initial rise up to the waiting point would make the waiting point more prominent even at higher accretion rates. Conversely, a slower reaction means that the reaction flow does not stop at any of the αp-process waiting points and hence no dip in the luminosity curve is observed.

However, while this occurs in some of the computed bursts, it does not occur in all the bursts due to compositional inertia. Therefore, while $^{18}\mathrm{Ne}(\alpha,p)^{21}\mathrm{Na}$ has an effect on the predicted x-ray burst light curves from spherically symmetric simulations, one-to-one comparisons with observations would be overly optimistic. More realistic 2D or even 3D model studies are clearly necessary to make more reliable predictions.

ACKNOWLEDGMENTS

This work was supported by the National Science Foundation under Grant No. PHY01-40324 and the Joint Institute for Nuclear Astrophysics, NSF-PFC, under Grant No. PHY02-16783. This work was partially performed under the auspices of the US Department of Energy by Lawrence Livermore National Laboratory under Contract DE-AC52-07NA27344. Also acknowledged is financial support from CONACyT and DGAPA, Mexico.

[1] S. E. Woosley and R. E. Taam, Nature **263**, 101 (1976).
[2] P. C. Joss, Nature **270**, 310 (1977).
[3] B. Lazareff, J. Audouze, S. Starrfield, and J. W. Truran, Astrophys. J. **228**, 875 (1979).
[4] M. Wiescher, J. Görres, and H. Schatz, J. Phys. G **25**, R133 (1999).
[5] R. K. Wallace and S. E. Woosley, Astrophys. J. **45**, 389 (1981).
[6] H. Schatz, A. Aprahamian, J. Görres, M. Wiescher, T. Rauscher, J. F. Rembges, F.-K. Thielemann, B. Pfeiffer, P. Möller, K.-L. Kratz *et al.*, Phys. Rep. **294**, 167 (1998).
[7] S. E. Woosley, A. Heger, A. Cumming, R. D. Hoffman, J. Pruet, T. Rauscher, J. L. Fisker, H. Schatz, B. A. Brown, and M. Wiescher, Astrophys. J. Suppl. **151**, 75 (2004).
[8] R. L. Cooper and R. Narayan, Astrophys. J. **648**, L123 (2006).
[9] J. L. Fisker, J. Görres, M. Wiescher, and B. Davids, Astrophys. J. **650**, 332 (2006).
[10] J. L. Fisker, W. Tan, J. Görres, M. Wiescher, and R. L. Cooper, Astrophys. J. **665**, 637 (2007).
[11] J. Fisker, H. Schatz, and F.-K. Thielemann, Astrophys. J. Suppl. **174**, 261 (2008).
[12] K. Langanke, M. Wiescher, W. A. Fowler, and J. Görres, Astrophys. J. **301**, 629 (1986).
[13] J. Görres, M. Wiescher, and F.-K. Thielemann, Phys. Rev. C **51**, 392 (1995).
[14] W. P. Tan, J. Görres, J. Daly, M. Couder, A. Couture, H. Y. Lee, E. Stech, E. Strandberg, C. Ugalde, and M. Wiescher, Phys. Rev. C **72**, 041302(R) (2005).
[15] R. Kanungo, T. K. Alexander, A. N. Andreyev, G. C. Ball, R. S. Charkrawarthy, M. Chicoine, R. Churchman, B. Davids, J. S. Forster, S. Guyrathi *et al.*, Phys. Rev. C **74**, 045803 (2006).
[16] W. P. Tan, J. L. Fisker, J. Görres, M. Couder, and M. Wiescher, Phys. Rev. Lett. **98**, 242503 (2007).
[17] F. Vanderbist, P. Leleux, C. Angulo, E. Casarejos, M. Couder, M. Loiselet, G. Ryckewaert, P. Descouvemont, M. Aliotta, T. Davinson *et al.*, Eur. Phys. J. A **27**, 183 (2006).
[18] A. A. Chen, R. Lewis, K. B. Swartz, D. W. Visser, and P. D. Parker, Phys. Rev. C **63**, 065807 (2001).
[19] J. A. Caggiano, W. Bradfield-Smith, J. P. Greene, R. Lewis, P. D. Parker, K. E. Rehm, and D. W. Visser, Phys. Rev. C **66**, 015804 (2002).
[20] G. P. A. Berg, K. Hatanaka, M. Wiescher, H. Schatz, T. Adachi, A. Bacher, C. Foster, Y. Fujita, H. Fujita, K. Fujita *et al.*, Nucl. Phys. **A718**, 608 (2003).
[21] W. Bradfield-Smith, T. Davinson, A. DiPietro, A. M. Laird, A. N. Ostrowski, A. C. Shotter, P. J. Woods, S. Cherubini, W. Galster, J. S. Graulich *et al.*, Phys. Rev. C **59**, 3402 (1999).
[22] D. Groombridge, A. C. Shotter, W. Bradfield-Smith, S. Cherubini, T. Davinson, A. D. Pietro, J. Görres, J. S. Graulich, A. M. Laird, P. Leleux *et al.*, Phys. Rev. C **66**, 055802 (2002).
[23] M. Fujiwara, H. Akimune, I. Daito, H. Fujimura, Y. Fujita, K. Hatanaka, H. Ikegami, I. Katayama, K. Nagayama, N. Matsuoka *et al.*, Nucl. Instrum. Methods A **422**, 484 (1999).
[24] J. Cseh, Phys. Lett. **B281**, 173 (1992).
[25] G. Lévai and J. Cseh, Ann. Phys. **230**, 165 (1994).
[26] T. Wakasa, K. Hatanaka, Y. Fujita, G. P. A. Berg, H. Fujimura, H. Fujita, M. Itoh, J. Kamiya, T. Kawabata, K. Nagayama *et al.*, Nucl. Instrum. Methods A **482**, 79 (2002).
[27] Y. Fujita, K. Hatanaka, G. P. A. Berg, K. Hosono, N. Matsuoka, S. Morinobu, T. Noro, M. Sato, K. Tamura, and H. Ueno, Nucl. Instrum. Methods B **126**, 274 (1997).
[28] H. Fujita, G. P. A. Berg, Y. Fujita, K. Hatanaka, T. Noro, E. J. Stephenson, C. C. Foster, H. Sakaguchi, M. Itoh, T. Taki *et al.*, Nucl. Instrum. Methods A **469**, 55 (2001).
[29] A. Matic, Ph.D. thesis, University of Groningen, 2007; http://dissertations.ub.rug.nl/faculties/science/2007/a.matic.
[30] D. Seweryniak, P. J. Woods, M. P. Carpenter, T. Davinson, R. V. F. Janssens, D. G. Jenkins, T. Lauritsen, C. J. Lister, C. Ruiz, J. Shergur *et al.*, Phys. Rev. Lett. **94**, 032501 (2005).
[31] N. Bateman, K. Abe, G. Ball, L. Buchmann, J. Chow, J. M. D'Auria, Y. Fuchi, C. Iliadis, H. Ishiyama, K. P. Jackson *et al.*, Phys. Rev. C **63**, 035803 (2001).
[32] P. M. Endt, Nucl. Phys. **A521**, 1 (1990).
[33] H. Fujita, Y. Fujita, G. Berg, A. Bacher, C. Foster, K. Hara, K. Hatanaka, T. Kawabata, T. Noro, H. Sakaguchi *et al.*, Nucl. Instrum. Methods A **484**, 17 (2002).
[34] M. Yosoi, http://www.rcnp.osaka-u.ac.jp/~yosoi/rcnpdaq_e.txt.
[35] http://www.nndc.bnl.gov/nudat2/.
[36] B. A. Brown, http://www.nscl.msu.edu/~brown/resources/resources.html.

[37] V. Z. Goldberg, G. V. Rogachev, W. H. Trzaska, J. J. Kolata, A. Andreyev, C. Angulo, M. J. G. Borge, S. Cherubini, G. Chubarian, G. Crowley *et al.*, Phys. Rev. C **69**, 024602 (2004).
[38] A. B. McDonald and E. G. Adelberger, Nucl. Phys. **A144**, 593 (1970).
[39] J. M. D'Auria, R. E. Azuma, S. Bishop, L. Buchmann, M. L. Chatterjee, A. A. Chen, S. Engel, D. Gigliotti, U. Greife, D. Hunter *et al.*, Phys. Rev. C **69**, 065803 (2004).
[40] C. Ruiz, T. Davinson, F. Sarazin, I. Roberts, A. Robinson, P. J. Woods, L. Buchmann, A. C. Shotter, P. Walden, N. M. Clarke *et al.*, Phys. Rev. C **71**, 025802 (2005).
[41] J. J. He, S. Kubono, T. Teranishi, M. Notani, H. Baba, S. Nishimura, J. Y. Moon, M. Nishimura, S. Michimasa, H. Iwasaki *et al.*, Eur. Phys. J. A **36**, 1 (2008).
[42] R. A. Paddock, Phys. Rev. C **5**, 485 (1972).
[43] W. P. Alford, P. Craig, D. A. Lind, R. S. Raymond, J. Ullman, C. D. Zafiratos, and B. H. Wildenthal, Nucl. Phys. **A457**, 317 (1986).
[44] K. Y. Chae, D. W. Bardayan, J. C. Blackmon, K. A. Chipps, R. Hatarik, K. L. Jones, R. L. Kozub, J. F. Liang, C. Matei, B. H. Moazen *et al.*, Phys. Rev. C **79**, 055804 (2009).
[45] N. Anantaraman, H. E. Gove, J. P. Trentelman, J. P. Draayer, and F. C. Jundt, Nucl. Phys. **A276**, 119 (1977).
[46] W. Scholz, P. Neogy, K. Bethge, and R. Middleton, Phys. Rev. C **6**, 893 (1972).
[47] U. Giesen, C. P. Browne, J. Görres, S. Graff, C. Iliadis, H. P. Trautvetter, M. Wiescher, V. Harms, K. L. Kratz, B. Pfeiffer *et al.*, Nucl. Phys. **A561**, 95 (1993).
[48] U. Giesen, C. Browne, J. Görres, J. Ross, M. Wiescher, R. Azuma, J. King, and M. Buckby, Nucl. Phys. **A567**, 146 (1994).
[49] S. Dababneh, M. Heil, F. Käppeler, J. Görres, M. Wiescher, R. Reifarth, and H. Leiste, Phys. Rev. C **68**, 025801(R) (2003).
[50] H. Trautvetter, M. Wiescher, K. Kettner, C. Rolfs, and J. Hammer, Nucl. Phys. **A297**, 489 (1988).
[51] C. E. Rolfs and W. S. Rodney, *Cauldrons in the Cosmos* (University of Chicago Press, Chicago, 1988).
[52] G. Lévai, J. Cseh, and W. Scheid, Phys. Rev. C **46**, 548 (1992).
[53] J. Cseh, G. Lévai, and W. Scheid, Phys. Rev. C **48**, 1724 (1993).
[54] G. Lévai and J. Cseh, Phys. Lett. **B381**, 1 (1996).
[55] Zs. Fülöp, G. Lévai, E. Somorjai, Á. Z. Kiss, J. Cseh, P. Tikkanen, and J. Keinonen, Nucl. Phys. **A604**, 286 (1996).
[56] J. Cseh, G. Lévai, A. Ventura, and L. Zuffi, Phys. Rev. C **58**, 2144 (1998).
[57] A. Lépine-Szily, M. S. Hussein, R. Lichtenthäler, J. Cseh, and G. Lévai, Phys. Rev. Lett. **82**, 3972 (1999).
[58] L. H. de la Peña, P. O. Hess, G. Lévai, and A. Algora, J. Phys. G **27**, 2019 (2001).
[59] P. O. Hess, A. Algora, J. Cseh, and J. P. Draayer, Phys. Rev. C **70**, 051303(R) (2004).
[60] J. Escher and J. P. Draayer, J. Math. Phys. **39**, 5123 (1998).
[61] J. P. Draayer, Nucl. Phys. **A237**, 157 (1975).
[62] K. T. Hecht, E. J. Reske, T. H. Seligman, and W. Zahn, Nucl. Phys. **A356**, 146 (1981).
[63] J. L. Fisker, F.-K. Thielemann, and M. Wiescher, Astrophys. J. **608**, L61 (2004).